Published in final edited form as:

Am J Med Genet A. 2021 September ; 185(9): 2719–2738. doi:10.1002/ajmg.a.62362.

Proximal variants in *CCND2* associated with microcephaly, short stature, and developmental delay: A case series and review of inverse brain growth phenotypes

Filomena Pirozzi[1], **Benson Lee**[2], **Nicole Horsley**[1], **Deepika D. Burkardt**[3], **William B. Dobyns**[4], **John M. Graham Jr**[5], **Maria L. Dentici**[6,7], **Claudia Cesario**[8], **Jens Schallner**[9], **Joseph Porrmann**[10], **Nataliya Di Donato**[10], **Pedro A. Sanchez-Lara**[5], **Ghayda M. Mirzaa**[1,11,12,13]

[1]Center for Integrative Brain Research, Seattle Children's Research Institute, Seattle, Washington, USA

[2]Division of Medical Genetics, Department of Medicine, Veterans Affairs Greater Los Angeles Healthcare System, Los Angeles, California, USA

[3]National Human Genome Research Institute, National Institutes of Health, Bethesda, Maryland, USA

[4]Division of Genetics and Metabolism, Department of Pediatrics, University of Minnesota, Minneapolis, Minnesota, USA

[5]Medical Genetics Institute, Cedars-Sinai Medical Center, David Geffen School of Medicine at UCLA, Los Angeles, California, USA

[6]Medical Genetics Unit, Academic Department of Pediatrics, Bambino Gesù Children's Hospital, IRCSS, Rome, Italy

[7]Genetics and Rare Diseases Research Division, Bambino Gesù Children's Hospital, IRCSS, Rome, Italy

[8]Translational Cytogenomics Research Unit, Bambino Gesù Children's Hospital, IRCCS, Rome, Italy

[9]Department of Neuropediatrics, School of Medicine, Carl Gustav Carus, TU Dresden, Dresden, Germany

Correspondence Filomena Pirozzi and Ghayda M. Mirzaa, Center for integrative Brain Research, Seattle Children's Research Institute, Seattle, WA, USA. filomena.pirozzi@seattlechildrens.org and ghayda.mirzaa@seattlechildrens.org.

AUTHOR CONTRIBUTIONS

Filomena Pirozzi and Ghayda M. Mirzaa conceptualized and designed the study, and analyzed all the clinical, molecular and functional data. Filomena Pirozzi performed western blot analysis, high-content imaging analysis, analyzed clinical and molecular data, and drafted the manuscript; Nicole Horsley performed cell culture, protein extraction, western blot experiments, and contributed to drafting of the manuscript; Benson Lee, Deepika D. Burkardt, William B. Dobyns, John M. Graham Jr., Maria L. Dentici, Claudia Cesario, Jens Schallner, Nataliya Di Donato, Pedro A. Sanchez-Lara, and Ghayda M. Mirzaa contributed to the acquisition of the data, drafting, and critical revision of the manuscript and associated data.

CONFLICT OF INTEREST

The authors declare no conflict of interest.

SUPPORTING INFORMATION

Additional supporting information may be found online in the Supporting Information section at the end of this article.

[10]Institute for Clinical Genetics, University Hospital, TU Dresden, Dresden, Germany

[11]Division of Medical Genetics, Department of Pediatrics, University of Washington, Seattle, Washington, USA

[12]Brotman-Baty Institute for Precision Medicine, Seattle, Washington, USA

[13]Institute for Stem Cell and Regenerative Medicine, University of Washington, Seattle, Washington, USA

Abstract

Cyclin D2 (CCND2) is a critical cell cycle regulator and key member of the cyclin D2-CDK4 (DC) complex. De novo variants of *CCND2* clustering in the distal part of the protein have been identified as pathogenic causes of brain overgrowth (megalencephaly, MEG) and severe cortical malformations in children including the megalencephaly-polymicrogyria-polydactyly-hydrocephalus (MPPH) syndrome. Megalencephaly-associated *CCND2* variants are localized to the terminal exon and result in accumulation of degradation-resistant protein. We identified five individuals from three unrelated families with novel variants in the proximal region of *CCND2* associated with microcephaly, mildly simplified cortical gyral pattern, symmetric short stature, and mild developmental delay. Identified variants include de novo frameshift variants and a dominantly inherited stop-gain variant segregating with the phenotype. This is the first reported association between proximal *CCND2* variants and microcephaly, to our knowledge. This series expands the phenotypic spectrum of *CCND2*-related disorders and suggests that distinct classes of *CCND2* variants are associated with reciprocal effects on human brain growth (microcephaly and megalencephaly due to possible loss or gain of protein function, respectively), adding to the growing paradigm of inverse phenotypes due to dysregulation of key brain growth genes.

Keywords

cyclin D2; inverse phenotypes; megalencephaly; megalencephaly-polymicrogyria-polydactyly-hydrocephalus syndrome (MPPH syndrome); microcephaly

1 | INTRODUCTION

Overgrowth syndromes are disorders characterized by cellular hyperplasia and/or hypertrophy, which may involve one or more of the three embryonic tissue layers (endoderm, ectoderm, or mesoderm) and present clinically with generalized or segmental overgrowth of the brain or the body (Burkardt et al., 2019; Tatton-Brown & Weksberg, 2013). Undergrowth syndromes or syndromes of growth restriction, on the other hand, are groups of disorders characterized by tissue hypoplasia and growth restriction. Collectively, these syndromes may manifest with localized or generalized growth abnormalities and display considerable heterogeneity in onset, tissue involvement and distribution among other features (Grissom & Reyes, 2013).

The Cyclin D2 Cyclin-dependent kinases 4 (CDK4) family of genes regulates the cell cycle by modulating the G1-to-S phase transition, critical for cell proliferation and development (Jeong et al., 2016). Posttranslational modification by phosphorylation of

CCND2, downstream of the phosphatidylinositol 3-kinase (PI3K)/ AK murine Thymoma (AKT)/mammalian target of the rapamycin (MTOR) signaling pathway inhibits its binding to the transcription factor E2F, allowing the cell to exit the G1 phase of the cell cycle (Becker et al., 2010; Bouchard et al., 1999; Sicinski et al., 1996). A schematic representation of the PI3K-AKT-MTOR pathway and CCND2 interaction is provided in Figure 1a. Cyclin D2 has well-studied roles in brain development and is expressed in dividing cells derived from neuronal precursors in the adult hippocampus (Ross et al., 1996). Hyperactivation of CCND2 has been linked to hematologic malignancies and increased proliferation in human cancer cell lines (Hung et al., 2018; Murai et al., 2001). Further, genetic variants of *CCND2* (MIM #123833), as well as two other key PI3K-AKT-MTOR pathway genes, namely *AKT3* and *PIK3R2*, have been identified as pathogenic causes of the megalencephaly-polymicrogyria-polydactyly-hydrocephalus (MPPH) syndrome (Hiraiwa et al., 2021; G. Mirzaa et al., 2014). MPPH is a rare megalencephaly (MEG) syndrome characterized by congenital or early postnatal brain overgrowth and cortical malformations, most commonly polymicrogyria (PMG). MPPH is also associated with variable degree of ventriculomegaly, with 40–50% of affected individuals progressing to hydrocephalus and necessitating surgical intervention (G. Mirzaa et al., 1993). Most affected children have mild to severe intellectual disability and oromotor dysfunction, including expressive language or speech delays, difficulties handling oral secretions, and dysphagia; with seizures reported in at least 50% of individuals. *CCND2*-related MPPH is characterized by severe and widespread polymicrogyria, typically bilateral perisylvian PMG (BPP) extending to the frontal and/or occipital lobes and correlating with increased severity of epilepsy and intellectual disability (G. Mirzaa et al., 2014). An additional report of a child with the MPPH phenotype in association with the *CCND2* variant, p.Thr280Ile, further expanded the phenotypic spectrum as this individual had additional brain abnormalities including hippocampal hypoplasia with malrotation, diffuse hypomyelination, and abnormalities of the midbrain and cerebellum (Cappuccio et al., 2019).

While overexpression and hyperactivation of CCND2 have been identified in humans and mice, the effects of CCND2 deficiency or loss of function have not been studied in humans. In mice, Ccnd2 knock-out leads to lack of cerebellar stellate interneurons (Garthe et al., 2014; Glickstein et al., 2007) and striking microcephaly (Huard et al., 1999). *CCND2* haploinsufficiency due to 12p13.32 contiguous microdeletion syndromes has been reported in individuals with microcephaly, although the critical region for this microdeletion also encompasses other key genes (Firth et al., 2009; Leyser et al., 2016). In this study, we describe three novel proximal variants in *CCND2* in five individuals from three unrelated families presenting with microcephaly, symmetric short stature, hypotonia and developmental delays. This series suggest that frameshift and stop-gain variants in the proximal portion of *CCND2* are linked to human microcephaly and adds *CCND2* to the growing list of genes associated with reciprocal brain growth dysregulation. All microcephaly- and megalencephaly (including MPPH)-associated variants in *CCND2* identified to date are schematically shown in Figure 1b. Examples of reciprocal gain and loss of protein function resulting in inverse phenotypes are seen in a multitude of abnormal growth syndromes, including mutations in other genes involved in cell growth and cell cycle regulation such as *AKT3*, *PTEN*, *NSD1*, and *MYCN*. These inverse brain growth

phenotypes due to reciprocal gene defects are summarized in Table 1 and discussed in depth in the literature review we provide here.

2 | METHODS

2.1 | Human subjects and cell lines

Families were identified through our clinical and research programs, personal communication, as well as the MatchMaker Exchange (MME) including GeneMatcher (http://www.genematcher.org) (Sobreira et al., 2015). Informed consent for publication and analysis of photos, imaging and clinical data was obtained from the patients' legal guardians under an IRB approved protocol at Seattle Children's Hospital (IRB#13291). Brain magnetic resonance imaging (MRI) studies were performed on three individuals (LR19–002, LR20–198a1, and LR20–198a2) and reviewed by the investigators. Fibroblast cell lines were established from one of the patients (LR19–392) with the c.305delG, p.G102Vfs*17 variant (referred to as LR19–392-MIC throughout the manuscript), and compared to a MEG/MPPH fibroblast cell line from a previously published patient (LR07–041) with the *CCND2*, c.839C>A, p.T280N variant (referred to as LR07–041-MEG hereon) (G. Mirzaa et al., 2014), as well as fibroblasts obtained from a healthy unrelated control (UW402–4-CTRL).

2.2 | Western blot analysis

Fibroblast cell lines (LR19–392-MIC, LR07–041-MEG, and UW402–4-CTRL) were expanded to six confluent T-75 flasks each before protein extraction. Cell culture flasks were placed on ice and washed once with 10 mL ice cold TBS. Flasks were then incubated on ice for 5 min with 500 μl cold RIPA buffer (Thermo Scientific, 89900) containing phosphatase and protease inhibitors (Thermo Scientific, 78,430, P5726, and P2850), cells were scraped and collected in 15 mL conical tubes and agitated for 30 minutes at 4C before being centrifuged at 14,000*g* for 15 min. The resulting supernatant was aliquoted into 0.2 mL tubes, snap frozen with liquid N2, and stored at −80°C. Protein concentrations were assessed via the standard Bicinchoninic Acid (BCA) Assay (Thermofisher, 23227). Equal amounts of protein extracts (10 and 20 μg) were heated to 95°C for 5 mins with NuPAGE® LDS Sample Buffer (4×) (Thermofisher, NP0007) and run on NuPAGE® Novex® 4–12% Bis-Tris gels (Thermofisher, NP0326BOX), together with a protein ladder (Pageruler prestained protein ladder, Thermofisher, 26617). Proteins were transferred to nitrocellulose membranes (Thermofisher, 77010). Due to low expression of CCND2 in human fibroblasts, we used 40 μg of protein extracts for its detection via Western Blot analysis. Membranes were blocked at room temperature for 1 h in blocking solution (3% BSA and 10% Donkey Serum in TBS with 0.1% Tween-20). For the CCND2 antibody, the blocking buffer contained 5% nonfat milk in addition to 3% BSA and 10% Donkey Serum to improve specificity. Membranes were incubated with primary antibody diluted in blocking solution overnight at 4C on an orbital shaker. Primary antibodies were diluted as follows: 1:200 for CCND2 (D52F9, Cell Signaling), 1:2500 for pAKT (Cell signaling, C31E5E), 1:2500 for pan-AKT (Cell Signaling, C67E7), 1:1000 for pS6 (Cell Signaling, 2215), and 1:5000 for β-actin (Abcam, ab8226). Membranes were washed three times for 15 min at room temperature in TBS-Tween 0.1% then incubated with secondary antibody in blocking solution for 1 h at RT. The secondary antibodies Donkey Anti-Mouse IgG H&L HRP (Abcam, ab205724) or

Donkey Anti-Rabbit IgG H&L HRP (Abcam, ab97064) were used at 1:10,000 in blocking solution. After three washes at room temperature with TBS-Tween 0.1%, protein signal was detected with Pierce™ ECL Western Blotting Substrate (Thermo Scientific, 32109) and visualized using a ChemiDoc-It®2810 Imager (Ultra-Violet Products Ltd., Cambridge, UK). If necessary, membranes were stripped and re-probed, probing the antibody for the protein with the weakest signal first, following standard protocols. Six independent experiments were performed for each antibody and images were analyzed, quantified, and normalized against B-Actin using ImageJ24. Statistical analysis and graphs were generated using GraphPad Prism version 9.0.2.

2.3 | High-content imaging

Fibroblast cell lines LR19–392 MIC, LR07–041 MEG, and UW402-CTRL were passaged in an optical 96 well plate coated with 0.1% porcine gelatin and cultured for 48 hours before fixing with cold 4% PFA in TBS (20 min at room temperature). Four wells per cell line were used for immunostaining. Cells were washed twice with cold TBS and permeabilized with TBS-Tween 0.1% for 5 min at room temperature. Immunostaining was performed using standard protocols. Briefly, cells were incubated for 1 hour at room temperature with blocking buffer (TBS-Tween 0.1% with 10% Donkey serum) and then incubated overnight with primary antibodies at 4C. Primary antibodies were diluted as follows: mouse anti-Ki-67 1:300 (Cell Signaling, 9449S) and rabbit anti-pS6 1:100 (Cell Signaling, 2215S). The following day, cells were washed three times with TBS-Tween 0.1% for 15 min and incubated with secondary antibodies diluted in blocking buffer for 1 h at room temperature. Secondary antibodies Donkey Anti-mouse Alexa 594 (Abcam, ab150112) and Donkey Anti-Rabbit Alexa 488 (Abcam, ab150065) and were used at 1:1000 dilution. Cells were washed three times in TBS-Tween 0.1%, followed by one wash in TBS, and stored in Glycerol-TBS (70:30) for acquisition and long-term storage. Image acquisition was performed using the CellInsight CX7 LZR system (Thermofisher). Fifteen fields for each of the 4 replicate wells per cell lines were acquired at 10× and 20× magnification. Images (10× magnification) were analyzed and quantified with a custom algorithm using the HCS Studio software. Statistical analysis was performed using GraphPad Prism version 9.0.2. and specific tests used are described in figure legends.

3 | RESULTS

3.1 | Clinical reports

Clinical and genetics features for all patients are summarized in Table 2.

3.1.1 | Patient LR19–002—This 7-month-old boy was referred to the genetics clinic for microcephaly, intrauterine growth restriction (IUGR), hypotonia, and mild motor delays. He was the first child of non-consanguineous parents of Armenian descent, a 30-year-old G1P1 mother and 30-year-old father and conceived by intrauterine insemination. Pregnancy was complicated by suspected preeclampsia and vaginal bleeding. No teratogenic exposures were reported. Family anamnesis was unremarkable with no history of microcephaly, delayed growth, or development. At 32–33 weeks of gestation, IUGR and placental insufficiency were reported. The boy was delivered at 35 + 5 weeks of gestation by a scheduled caesarian

section. Birth weight was 1870 grams (2nd centile, −2.05 SD), length 42.5 cm (3rd centile, −1.8 SD) and occipitofrontal circumference (OFC) 30.5 cm (3–10th centile, − 1–2 SD). OFC measured again at 36 weeks was 29.9 cm (1–2nd centile, −2.25 SD). The child was also diagnosed with gastroesophageal reflux and allergic colitis. At age 7 months, he was sitting up without assistance, had begun rolling in both directions, grabbed objects with both hands and was beginning to vocalize sounds. OFC was 40.2 cm (<1st centile, − 3.1 SD), weight was 6.1 kg (<1st centile, −2.6 SD), and length was 64.5 cm (5th centile, −1.6 SD). His body habitus was proportionately small with symmetric limbs, clinically apparent microcephaly with mild right occipital flattening but otherwise normal skull shape and no other notable dysmorphic features.

Brain magnetic resonance imaging (MRI) without contrast performed at age 6 months revealed apparent microcephaly with a diffusely simplified gyral pattern (Figure 2a–c). An echocardiogram performed at age 4 months revealed a small patent foramen ovale versus secundum atrial septal defect with left to right shunting.

Chromosomal microarray analysis was normal. Trio exome sequencing on buccal samples identified a heterozygous de novo variant in *CCND2* (NM_001759.4:c.416_419dupGGGA, p.L141GfsX19) (Figure 1b). This frameshift variant causes a premature stop codon at position 19 of the new reading frame and is predicted to cause a loss of normal protein function either through protein truncation or nonsense-mediated mRNA decay. This novel variant has not been observed in over 60,000 apparently normal individuals (Lek et al., 2016) (Table 3). Other reported findings unrelated to the patient's phenotype include a heterozygous paternally-inherited variant of uncertain significance (VUS) in *GBA* (NM_000157.4: c.882T>G, p.H294Q), and a maternally inherited hemizygous VUS in *TENM1* (NM_001163278.1:c.679 C>A, p.P227T) a gene not currently known to be associated with microcephaly or other human Mendelian disorders, but has been reported as possibly associated with cerebral palsy (McMichael et al., 2015), autism spectrum disorder (Yuen et al., 2015), schizophrenia (Gulsuner et al., 2013), and congenital general anosmia (Alkelai et al., 2016).

3.1.2 | Patient LR19–392—This 12-year-old girl presented with a history of IUGR, microcephaly, delayed language skills, mild attention deficit hyperactivity disorder (ADHD), and short stature. She was the second child born to non-consanguineous parents. Family history was unremarkable with no microcephaly, growth, or developmental delay. Pregnancy was uneventful until the end of the second trimester when IUGR was identified. Amniocentesis revealed a normal female karyotype (46,XX). She was delivered at 39 weeks of gestation by scheduled cesarean section due to IUGR. Her birth weight was 2320 grams (3rd centile, − 1.8 SD), length was 46 cm (3–10th centile, −1.5 SD), and OFC was 32 cm (2nd centile, −2 SD). At age 2 years and 10 months, her weight was 9.8 kg (<1st centile, −2.8 SD), length was 89 cm (18th centile, −0.93 SD), and OFC was 43.6 cm (<1st centile, −3.1 SD). Bone age was delayed by 6 months but normalized at later follow-up. Evaluation of growth hormone response to GHRH plus arginine at 8 years of age was normal.

Her motor developmental milestones were within the normal range. She sat without assistance at age 6–7 months and walked unsupported at age13 months. Her language skills

were delayed. She had mild attention deficit hyperactivity disorder (ADHD) and attended a special education program at school. Vision assessment revealed mild myopia. At her last evaluation at 12 years and 2 months, weight was 25.50 kg (<1st centile, −2.8 SD), height 140.50 cm (8th centile, −1.42 SD) and OFC was 48 cm (<1st centile, −4.27 SD). Physical examination revealed marked microcephaly with relatively large ears, short philtrum, and an incomplete right single transverse palmar crease.

Head ultrasound performed at birth did not show any structural abnormalities. A brain MRI has not been performed due to the presence of dental braces. An electroencephalogram (EEG) was performed at 12 years and 5 months and was normal.

Targeted multigene NGS panel testing for microcephaly using the NimbleGen SeqCap Target Enrichment kit (Roche) by NextSeq550 Platform (Illumina) revealed a heterozygous de novo variant in *CCND2* (NM_001759.4:c.305delG). This single base deletion is expected to cause a premature stop codon, p.G102Vfsx17 (Figure 1b), with the de novo status confirmed by segregation analysis performed by Sanger sequencing of both parents. This novel variant was not observed in large population cohorts (Table 3). Other microcephaly genes in the panel include *MCPH1*, *WDR62*, *CDK5RAP2*, *CASC5*, *ASPM*, *CENPJ*, *STIL*, *CEP135*, *CEP152*, *CDK6*, *ATR*, *RBBP8*, *CEP63*, *NIN*, and *ATRIP*.

3.1.3 | Family LR20–198—This family includes two siblings: a 12-year-old boy (LR20–198a1) and 6-year-old girl (LR20–198a2) born to their 30-year-old mother (LR20–198 m). LR20–198a1 presented prenatally with IUGR and microcephaly. He was born at 38 + 5 weeks of gestation by emergency cesarean section and had severe perinatal asphyxia (Apgar scores of 1, 6, and 9 at 1, 5, and 10 min, respectively). Developmental delay was documented at the age of 3 years. The child attends special education classes at school and has abnormal behaviors with frequent temper tantrums and aggression. A brain MRI at the age of 4 years shows mildly foreshortened frontal lobes and very subtle simplification of the cortical gyral pattern. Brain MR images and clinical photographs are shown in Figure 2d–h. The younger sister, LR20–198a2, similarly presented with IUGR. Microcephaly was documented at the age of 12 months. She also had short stature from the 2nd year of life, with failure to thrive, feeding difficulties and speech delays. At the age of 4 years, she had several seizure-like episodes and an abnormal EEG pattern, but no anti-epileptic treatments were initiated. A brain MRI performed at age 2 years and 5 months was normal. Brain MR images and clinical photographs are shown in Figure 2i–m. The mother of these two siblings, LR20–198 m, also had microcephaly (OFC 51 cm <1st centile, − 3.1 SD) and had short stature (height 150 cm, 2nd centile, −2 SD). She was also identified to have mild intellectual and learning disabilities. She attended special education classes at school and did not graduate. Her health history was otherwise unremarkable.

Exome sequencing performed on LR20–198a1 showed a heterozygous *CCND2* variant (NM_001759.4:c.544C>T, p.Q182X) which was not observed in gnomADv2.1.1 or in-house databases. This nonsense variant is predicted to be deleterious by in silico prediction programs including Combined Annotation Dependent Depletion (CADD) and Mutation Taster (Kircher et al., 2014; Schwarz et al., 2014). Through targeted sequencing, this variant was confirmed in the heterozygous state in both LR20–198a2 and LR20–198 m

but was absent in three unaffected siblings. A chromosomal microarray on LR20–198a1 demonstrated an 85 kb intragenic microduplication affecting exons 20–25 of *PIK3C3*. This microduplication was present in LR20–198a2 and LR20–198 m but also in several unaffected relatives and was therefore considered to be benign.

Table 2 summarizes the clinical features and molecular features of the five individuals in this series. We investigated the potential pathogenicity of the three *CCND2* variants, as well as the *TNEM1* variant identified in individual LR19–002 using several in silico prediction programs. All *CCND2* variants were classified as disease causing and were not present in public databases such as dbSNP, 1000Genomes and gnomADv2.1.1 (Auton et al., 2015; Karczewski et al., 2020; Sherry et al., 2001). These results are summarized in Table 3. In gnomAD, coverage of the regions surrounding the three novel *CCND2* variants reported here was good (gnomADv2.1.1, over 240,000 reference alleles), and seven putative loss of function (pLoF) variants are listed in the gene. However, none of them overlap with our variants, six of these are classified as low confidence (variant annotation or quality dubious) pLoF calls, with the remaining pLoF variant, p.Glu272Ter, listed as pathogenic.

3.2 | Western blot analysis of CCND2 mutant fibroblasts

To identify differences in CCND2 expression levels and compare them to expression levels of proteins in the PI3K-AKT-MTOR pathway, including AKT, phosphorylated AKT (pAKT), and phosphorylated S6 (pS6), we performed western blot experiments using protein extracts from control fibroblasts (UW402–4-CTRL), one *CCND2* MEG patient (LR07–041-MEG, p.T280N) and one *CCND2* MIC patient (LR19–392-MIC, p.G102VfsX17). Due to low expression of CCND2 in primary human fibroblasts, we confirmed the specificity of the CCND2 antibody band at 31KDa using a mouse cerebellar protein extract (Supplementary Figure 1A). When compared to the control human fibroblast cell line, the LR07–041-MEG line had significantly increased levels of CCND2 (average 1.6-fold change) as well as increased levels of panAKT (average 1.71-fold change), pAKT (1.64-fold change) and pS6 (2.41-fold change), as expected (Figure 3a–c, Supplementary Table 1, Supplementary Figure 1C). Interestingly, the LR19–392-MIC line also had significantly increased levels of CCND2 compared to controls (average 1.17-fold change). The increase in CCND2 correlated with a small increase in pS6 levels (average 1.16-fold change), but not of panAKT or pAKT (Figure 3a–c, Supplementary Table 1, Supplementary Figure 1C).

3.3 | High-content imaging of CCND2 mutant fibroblasts

To assess the morphological and functional differences between LR19–392-MIC and LR07–041-MEG cell lines, we performed immunostaining of key markers for proliferation (Ki-67) and MTOR hyperactivation (pS6) using high-content imaging performed with the CellInsight CX7 LZR (Thermofisher). We analyzed 33,218 cells in total for UW402–4-CTRL line; 36,104 cells for the LR19–392-MIC line; and 12,508 cells for the LR07–041-MEG line, as shown in Figure 4. We identified a significant increase in the percentage of pS6 positively staining cells in LR07–041-MEG, but not in LR19–392-MIC cells (Figure 4). The increase in pS6+ cells was accompanied by a significant increase in the percentage of double positive cells (pS6+/Ki-67 +) in LR07–041-MEG. In addition, the intensity

(and thus the levels of expression) of both pS6 and Ki-67 were significantly higher in LR07–041-MEG but not in LR19–392-MIC (Figure 4). More interestingly, cytoplasmic area assessments via pS6 staining revealed marked hypertrophy in LR07–041-MEG cells (average area 590.93 pixel^2) compared to controls and to the LR19–392-MIC line (376.18 pixel^2 in UW402–4, and 329.13 pixel^2 in LR19–392) (Figure 4b).

3.4 | Literature review of reciprocal brain growth phenotypes

In light of our findings, we reviewed the literature of inverse brain phenotypes similar to *CCND2* associated with reciprocal functional effects of genes. A brief overview of these genes, namely *AKT3*, *PTEN*, *NSD1*, *MYCN*, *EZH2*, and *MIR17HG*, is provided below, and their associated phenotypes are summarized in Table 1.

AKT3—*AKT3*, also known as protein kinase B (PKB), is located on chromosome 1q43–44 and encodes a serine/threonine protein kinase expressed primarily in the brain. *AKT3* is one of three closely related AKT isoforms and is the primary downstream effector of PI3K signaling. PI3K-AKT-mTOR signaling regulates many important cell functions, including protein synthesis, cell proliferation and survival (Diez et al., 2012; Ersahin et al., 2015; Ling Wang et al., 2017). *AKT3* exerts its regulatory effects through serine and/or threonine phosphorylation of various downstream substrates, one of which is linked to influencing cyclin-D2 levels by S9 residue phosphorylation and subsequent inactivation of glycogen synthase kinase-3 β (GSK-3β) (P. Cohen & Frame, 2001; Hermida et al., 2017; Miao et al., 2016; Ouimet et al., 2019). GSK-3β is a negative regulator of cyclin D1 and D2 by ubiquitin dependent degradation. The AKT family of proteins are implicated in a wide range of human diseases including cancer, diabetes, cardiovascular and neurological disease (Alcantara et al., 2017; Chung et al., 2014; Conti et al., 2015; Dobyns & Mirzaa, 2019; Gai et al., 2015; Grabinski et al., 2011; Hers et al., 2011; Lee et al., 2012; Lopes et al., 2019; Mure et al., 2010; Poduri et al., 2012; Riviere et al., 2012; D. Wang et al., 2013; Yang et al., 2005). Gain-of-function variants in *AKT3* lead to inactivation of GSK-3β which in turn results in stabilization and increased levels of cyclin D2 which has been proposed as the unifying mechanism for MPPH syndrome (G. Mirzaa et al., 2014). Data from humans and animal models suggest a gene dosage effect of *AKT3* resulting in inverse phenotypes. *Akt3* knockout mice display microcephaly suggesting that it plays a critical role in determining brain size (Easton et al., 2005; Yang et al., 2005). Mosaic and constitutional gain-of-function variants of *AKT3* are associated with MPPH syndrome (Lee et al., 2012; Lopes et al., 2019; Poduri et al., 2012; Riviere et al., 2012), with more than 20 patients reported to date with molecularly confirmed *AKT3* related megalencephaly (Alcantara et al., 2017; Harada et al., 2015; Jamuar et al., 2014; Nakamura et al., 2014; Negishi et al., 2017; Nellist et al., 2015; Riviere et al., 2012). A subset of affected individuals is mosaic for the common p.E17K mutation causing hemimegalencephaly (Jansen et al., 2015; Lee et al., 2012; Poduri et al., 2012; Riviere et al., 2012). Duplications of 1q43-q44 encompassing *AKT3* have also been reported to cause macrocephaly (Chung et al., 2014; Hemming et al., 2016; Luo et al., 2018; D. Wang et al., 2013). Heterozygous deletions of 1q43-q44 involving *AKT3*, on the other hand, result in postnatal microcephaly and agenesis of the corpus callosum (Gai et al., 2015; Hemming et al., 2016; Lopes et al., 2019).

PTEN—Loss-of-function variants in *PTEN*, which encodes for phosphatase and tensin homolog and tumor suppressor, cause a spectrum of clinical megalencephaly disorders including Cowden syndrome (CS), Bannayan–Riley–Ruvalcaba syndrome (BRRS), and autism spectrum disorder with macrocephaly (Gorlin et al., 1992; Herman et al., 2007; Marsh et al., 1998; Orrico et al., 2009; Varga et al., 2009; Zhou et al., 2003). These syndromes share characteristic features including overgrowth and predisposition to various tumors. PTEN suppresses phosphoinositide 3-kinase (PI3K) signaling that activates cell growth and tumorigenesis. Mice deficient in nuclear PTEN have microcephaly persisting into adulthood (Igarashi et al., 2018; Kwon et al., 2001; Kwon et al., 2003; Kwon et al., 2006). Further, deletions of the 10q23 locus encompassing *PTEN* are associated with macrocephaly, hypotonia, and increased predisposition to various malignancies, including juvenile polyposis syndrome (Babovic et al., 2010). In contrast, microduplications of this locus have recently been identified in association with autosomal dominant primary microcephaly and decreased mTOR signaling (Oliveira et al., 2019).

NSD1—*NSD1*, located on chromosome 5q35.3, encodes for nuclear receptor binding (SET) domain histone methyltransferase that methylates lysine 36 of histone 3 (H3K36) (Graham et al., 2016). This histone modifier regulates the activity of several genes involved in growth and development. Haploinsufficiency of *NSD1* causes Sotos syndrome characterized by brain and somatic overgrowth, distinctive facial features (broad, prominent forehead, dolichocephaly, spares frontotemporal hair, long chin, long narrow face, malar flushing, down-slanting palpebral fissures), and intellectual disability (Kurotaki et al., 2002). Other major features include behavioral problems, advanced bone age, cardiac defects, cranial abnormalities, skeletal abnormalities including joint hyperlaxity and scoliosis, renal defects, and seizures. A minority of affected individuals (<15%) have other features such as hemihypertrophy, conductive hearing loss, pectus excavatum, and strabismus. Loss-of-function variants and deletions of 5q35 encompassing *NSD1* have been identified in approximately 90% of individuals with Sotos syndrome (Tatton-Brown et al., 2005). Conversely, *NSD1* duplications result in growth retardation and microcephaly (Dikow et al., 2013; Franco et al., 2010; Lucio-Eterovic et al., 2010; Sachwitz et al., 2017; Sellars et al., 2011; Tracy et al., 2011; J. C. Wang et al., 2007; Zhang et al., 2011). Further, murine models carrying a heterozygous 1.5-Mb deletion of 36 genes including *Nsd1* syntenic with 5q35.2-q35.3 in humans had a phenotype characterized by small gestational age and decreased postnatal growth (Migdalska et al., 2012).

MYCN—*MYCN*, located on chromosome 2p24.3, encodes for N-Myc protein, a transcription factor critical to normal embryonic development and postnatal brain size. The *MYCN* gene is part of the Myc family of proto-oncogenes critical for regulating cell differentiation and growth (Henriksson & Luscher, 1996). Much of the function of the Myc family of proteins is through downstream activation and repression of specific target genes (Eisenman, 2001). These targets include the cyclin-dependent kinase *CDK4*, a Cdc25A phosphatase that activates CDKs, cyclin D2 and the E2F family (Bouchard et al., 1999; Galaktionov et al., 1996; Leone et al., 2001). Amplification of *MYCN* is associated with various cancers including prostate cancer (Dardenne et al., 2016), retinoblastoma (Rushlow et al., 2013), and aggressive forms of neuroblastoma (Higashi et al., 2019; Otto et al.,

2009; Tavana et al., 2016; Xue et al., 2016). The carcinogenic potential of N-Myc is likely due to its ability to drive cells into the cell cycle. A mouse model showed that *N-myc* plays a vital role in neurogenesis and that homozygous absence of *N-myc* results in a twofold decrease in brain mass that disproportionately affects the cerebellum and cerebral cortex (Knoepfler et al., 2002). This same study suggested that the decrease in brain size is due to downregulation of a subset of cyclin-dependent kinase inhibitors and disruption of *CCND2* expression. Germline loss of function variants of *MYCN* cause Feingold syndrome type 1 characterized by microcephaly, limb abnormalities, atresia of the gastrointestinal tract, learning disabilities, and dysmorphic facial features. Deletions involving the *MYCN* locus have also been reported as a cause of Feingold Syndrome (Chen et al., 2012; Mercedes Bloch et al., 2014). Although there is variable expressivity, there are no significant genotype–phenotype differences between individuals with Feingold Syndrome (Marcelis et al., 2008). Further, an *MYCN* gain-of-function variant resulting in increased *CCND1* and *CCND2* expression has recently been reported to cause a novel megalencephaly syndrome that is similar but distinct from MPPH syndrome (Kato et al., 2018).

EZH2—Enhancer of Zeste, Drosophila, homolog 2 (*EZH2*, MIM: 601573) encodes for part of the polycomb repressive complex 2 (PRC2), which mediates suppression of transcription via chromatin condensation through methylation of histone H3 (lysine 27) (Cao et al., 2002). Variants in this gene are the primary cause of Weaver Syndrome (WS), characterized by overgrowth, facial gestalt, accelerated bone maturation and variable degree of intellectual disability (A. S. Cohen et al., 2016; Gibson et al., 2012; Lui et al., 2018; Tatton-Brown et al., 2011; Tatton-Brown et al., 2013). Studies in humans and mice have demonstrated that *EZH2* variants associated with WS are mainly due to reduced methyltransferase activity, and thus are classified as loss of function (A. S. Cohen & Gibson, 2016; Lui et al., 2018). Recently, an elegant study utilized DNA methylation signature to classify missense variants in *EZH2* as pathogenic or benign, and provided insights into gain of function mutations and mosaicism (Choufani et al., 2020). Notably, gain of methylation at the same CpG sites associated with WS, lead to transcriptional changes during development resulting in growth restriction in one patient (Choufani et al., 2020). This evidence adds *EZH2* to the growing list of genes with epigenetic functions that can affect cell growth through changes in their transcriptional profiles, similarly to *NSD1* (Aref-Eshghi et al., 2018; Butcher et al., 2017; Choufani et al., 2015).

MIR17HG* and 13q31.3—MIR17HG* gene encodes the miR-17 ~92 polycistronic microRNA (miRNA) cluster, a family of six highly conserved miRNA (Han et al., 2015). Focal amplifications of this region are present in many types of cancer, with ectopic expression of this locus associated with acceleration of tumor formation in murine models (Han et al., 2015). Microdeletions of chromosome 13q that include the *MIR17HG* gene are associated with Feingold 2 syndrome, with features of microcephaly, brachymesophalangy, toe syndactyly, short stature, cardiac anomalies, growth hormone deficiency, aortic dilation, phalangeal joint contractures, memory, and sleep problems (de Pontual et al., 2011; Muriello et al., 2019). Recently, a de novo 13q31.3 microduplication encompassing *MIR17HG* was described in a female patient with developmental delay, skeletal and digital abnormalities, and tall stature and macrocephaly (Siavriene et al., 2020).

4 | DISCUSSION

The *CCND2* gene, located on 12p13.32, encodes the protein Cyclin D2 and is a member of the highly conserved cyclin family, regulating the G1 to S phase transition in the cell cycle (Z. Wang et al., 2008; Xiong et al., 1992). Gain-of-function (GoF) variants in *CCND2*, *AKT3* and *PIK3R2* have been implicated in MPPH syndrome. Megalencephaly-associated variants in components of the PI3K-AKT-MTOR pathway, including variants within the terminal exon of *CCND2*, share the same functional endpoint, namely inhibition of proteasomal degradation of cyclin D2 (G. Mirzaa et al., 2014). This influences many important cell functions including cell growth and division, protein synthesis and cell survival. Although not directly in the PI3K-AKT-MTOR pathway, *MCYN* indirectly participates through upstream modulation of *CCND1* and *CCND2* expression (Kato et al., 2018). Further, copy number abnormalities, namely 12p13.32 deletions encompassing *CCND2*, have been identified in individuals with microcephaly and a wide spectrum of clinical features including intellectual disability, short stature, developmental delays, and dysmorphic features. However, the highly variable presentation and high gene content of this microdeletion syndrome provided limited evidence regarding the role of *CCND2*. (Firth et al., 2009). This is the first series reporting on individuals with heterozygous frameshift and stop gain *CCND2* variants resulting in microcephaly, to our knowledge. All affected individuals demonstrated poor growth, in association with neurodevelopmental issues, among other features.

CCND2 is highly expressed in pluripotent human embryonic stem cells (Becker et al., 2010), and is postnatally expressed at high levels in the human brain, adrenal gland, heart, and colon (Fagerberg et al., 2014). CCND2 is a regulatory subunit of the Cyclin D2-CDK4 complex, which phosphorylates and inhibits members of the retinoblastoma (RB) family of proteins including RB1. Phosphorylation of RB1 allows dissociation of the transcription factor E2F from the RB/E2F complex and the subsequent transcription of E2F target genes responsible for progression through the G1 phase of the cell cycle. Cyclin D2 is also a substrate for SMAD3, phosphorylating SMAD3 in a cell-cycle-dependent manner and repressing its transcriptional activity. Cyclin D2 has been found to be highly expressed in the adult mouse brain suggesting that cyclin D2 carries out a unique role in terminally differentiated neurons (Ross et al., 1996). Murine knockout models of *Ccnd2* lack adult neurogenesis almost entirely (Kondratiuk et al., 2015). A deficit in parvalbumin positive (PV+) GABAergic interneurons in *Ccnd2* null mice have been observed in both the cortex and the hippocampus leading to a decrease in cortical inhibition (Glickstein et al., 2007). Evidence of this cortical inhibition was demonstrated on EEGs of awake *cD2*-null mice showing increased frequency and amplitude of paroxysmal cortical discharges (Glickstein et al., 2007). Furthermore, gene dose dependent differences in brain cortical surface area have been observed in mouse models with heterozygous knockouts of *Ccnd2* resulting in an intermediate phenotype (Glickstein et al., 2007). *Ccnd2* null mice had microcephaly with either a relatively preserved or mildly decreased body size with catch up growth and an increase in seizure activity as they age (M. Elizabeth Ross, personal communication, April 25, 2019).

Our series of five individuals with microcephaly and three novel variants in *CCND2* expands the genotype–phenotype spectrum for this gene. Our functional analysis revealed increased levels of CCND2 and other key PI3K-AKT-MTOR markers in *CCND2* mutant fibroblasts derived from a child with MPPH, confirming previous findings by our group (G. Mirzaa et al., 2014). Immunostaining also revealed marked increase in Ki-67 expression, suggesting that increased proliferation is a mechanism for CCND2-related MEG, as demonstrated by our prior work on *CCND2* (G. Mirzaa et al., 2014). Our data further show that an increase in cell size, or cellular hypertrophy, is likely another feature of *CCND2*-related MEG, as demonstrated by the significant enlargement of cytoplasmic area, and similar to the MTOR-dependent hypertrophy identified in *Pten*-deficient mice (Kwon et al., 2001; Kwon et al., 2003). Despite the increase in pS6+ and Ki-67+/pS6+ cells, the LR07–041 MEG cell line showed a reduced overall percentage of Ki67+ cells, due to the overall lower number of cells present in the wells, as cells occupy a larger volume (12,508 cells for LR07–041 MEG vs. 33,218 cells in the control). Similar assays on the *CCND2*-associated microcephaly cell line revealed lower levels of *CCND2* compared to the MEG cell line. However, levels were surprisingly slightly higher than the control line. We were able to detect the CCND2 protein in the LR19–392 MIC cell line despite the premature stop codon as the antibody recognized an epitope in the N-terminus, suggesting expression of a truncated isoform of the protein in this patient. We therefore hypothesize that the increase in CCND2 levels in the MIC cell line could be due to accumulation of unphosphorylated degradation-resistant cyclin D2, similarly to what demonstrated for *CCND2* -related MPPH (G. Mirzaa et al., 2014), albeit with distinct functional consequences in the developing brain. We also hypothesize that this mild increase in protein level is likely insufficient to cause hyperplasia or hypertrophy, as the LR19–392-MIC cells were not significantly different in size or number from controls. We previously identified a nonsense variant in the terminal exon of *CCND2* in association with MPPH (p.Lys270X) (G. Mirzaa et al., 2014), thus we postulate that variants in distinct regions of the gene (proximal vs. distal) are directly relevant to the functional consequences and associated phenotypes of *CCND2*-related disorders.

We considered whether the *TENM1* hemizygous variant in individual LR19–002 could contribute to the phenotype. However, we believe this is less likely as *TENM1* is not known to be associated with microcephaly, to date. Notably, individual LR19–392 in our study underwent only targeted multigene sequencing. Therefore, we cannot rule out the possibility that this individual may carry other variants that might contribute to the phenotype. Finally, additional functional studies in more relevant models, such as human induced pluripotent stem cell-derived neurons, are needed to confirm some of the above hypotheses regarding the role of *CCND2* in regulating brain size and the exact molecular mechanisms of *CCND2*-related microcephaly in humans.

In summary, our study expands the phenotypic spectrum of *CCND2*-related disorders in humans and suggests that distinct classes of genetic variants within different domains of the gene—namely proximal versus distal variants—have different functional consequences on the developing human brain and are likely associated with reciprocal effects on early brain growth—with more proximal and potentially loss of function variants causing protein truncation associated with microcephaly, and distal variants abolishing phosphorylation-dependent ubiquitination sites resulting in megalencephaly. This study further highlights the

diversity of the molecular mechanisms that cause brain growth syndromes and the paradigm of reciprocal genetic variants leading to inverse brain phenotypes.

Supplementary Material

Refer to Web version on PubMed Central for supplementary material.

ACKNOWLEDGMENTS

We thank the patients, their families and care providers for their contribution to this study. We thank Dr. M. Elizabeth Ross, Professor of Neurology and Neuroscience, and the Ross Laboratory at Weill Cornell Medicine for their expert input regarding the function and role of CCND2 in brain development. We also thank Dr. Daniel Doherty, Professor of Pediatrics and Developmental Medicine, for providing the control fibroblast cell line used in this manuscript (UW402-4). Research reported in this publication was supported by Jordan's Guardian Angels and the Sunderland Foundation (to Filomena Pirozzi and Ghayda M. Mirzaa), and the Brotman-Baty Institute (to Ghayda M. Mirzaa); Nataliya Di Donato work was supported by German Research Foundation (DI 2170/3-1). The content is solely the responsibility of the authors and does not necessarily represent the official views of the National Institutes of Health. The funding sources had no role in the design and conduct of the study, collection, management, analysis and interpretation of the data, preparation, review or approval of the manuscript, or decision to submit the manuscript for publication.

Funding information

Brotman-Baty Institute; German Research Foundation, Grant/Award Number: DI 2170/3-1; Jordan's Guardian Angels; Sunderland Foundation

DATA AVAILABILITY STATEMENT

The authors confirm that the data supporting the findings of this study are available within the article and its supplementary material. The raw data that support the findings of this study, including the genetic analyses and the high content imaging results are available on request to the corresponding authors.

REFERENCES

Alcantara D, Timms AE, Gripp K, Baker L, Park K, Collins S, Cheng C, Stewart F, Mehta SG, Saggar A, Sztriha L, Zombor M, Caluseriu O, Mesterman R, Van Allen MI, Jacquinet A, Ygberg S, Bernstein JA, Wenger AM, … Mirzaa GM (2017). Mutations of AKT3 are associated with a wide spectrum of developmental disorders including extreme megalencephaly. Brain, 140(10), 2610–2622. 10.1093/brain/awx203 [PubMed: 28969385]

Alkelai A, Olender T, Haffner-Krausz R, Tsoory MM, Boyko V, Tatarskyy P, Gross-Isseroff R, Milgrom R, Shushan S, Blau I, Cohn E, Beeri R, Levy-Lahad E, Pras E, & Lancet D (2016). A role for TENM1 mutations in congenital general anosmia. Clinical Genetics, 90(3), 211–219. 10.1111/cge.12782 [PubMed: 27040985]

Aref-Eshghi E, Rodenhiser DI, Schenkel LC, Lin H, Skinner C, Ainsworth P, Paré G, Hood RL, Bulman DE, Kernohan KD, Care4Rare Canada Consortium, Boycott KM, Campeau PM, Schwartz C, & Sadikovic B (2018). Genomic DNA methylation signatures enable concurrent diagnosis and clinical genetic variant classification in neurodevelopmental syndromes. American Journal of Human Genetics, 102(1), 156–174. 10.1016/j.ajhg.2017.12.008 [PubMed: 29304373]

Auton A, Brooks LD, Durbin RM, Garrison EP, Kang HM, Korbel JO, Marchini JL, McCarthy S, McVean GA, Abecasis GR, & Genomes Project C (2015). A global reference for human genetic variation. Nature, 526(7571), 68–74. 10.1038/nature15393 [PubMed: 26432245]

Babovic N, Simmons PS, Moir C, Thorland EC, Scheithauer B, Gliem TJ, & Babovic-Vuksanovic D (2010). Mucinous cystadenoma of ovary in a patient with juvenile polyposis due to 10q23

microdeletion: Expansion of phenotype. American Journal of Medical Genetics. Part A, 152A(10), 2623–2627. 10.1002/ajmg.a.33637 [PubMed: 20815035]

Becker KA, Ghule PN, Lian JB, Stein JL, van Wijnen AJ, & Stein GS (2010). Cyclin D2 and the CDK substrate p220(NPAT) are required for self-renewal of human embryonic stem cells. Journal of Cellular Physiology, 222(2), 456–464. 10.1002/jcp.21967 [PubMed: 19890848]

Bouchard C, Thieke K, Maier A, Saffrich R, Hanley-Hyde J, Ansorge W, Reed S, Sicinski P, Bartek J, & Eilers M (1999). Direct induction of cyclin D2 by Myc contributes to cell cycle progression and sequestration of p27. The EMBO Journal, 18(19), 5321–5333. 10.1093/emboj/18.19.5321 [PubMed: 10508165]

Burkardt DD, Tatton-Brown K, Dobyns W, & Graham JM Jr. (2019). Approach to overgrowth syndromes in the genome era. American Journal of Medical Genetics. Part C, Seminars in Medical Genetics, 181(4), 483–490. 10.1002/ajmg.c.31757

Butcher DT, Cytrynbaum C, Turinsky AL, Siu MT, Inbar-Feigenberg M, Mendoza-Londono R, Chitayat D, Walker S, Machado J, Caluseriu O, Dupuis L, Grafodatskaya D, Reardon W, Gilbert-Dussardier B, Verloes A, Bilan F, Milunsky JM, Basran R, Papsin B, … Weksberg R (2017). CHARGE and kabuki syndromes: Gene-specific DNA methylation signatures identify epigenetic mechanisms linking these clinically overlapping conditions. American Journal of Human Genetics, 100(5), 773–788. 10.1016/j.ajhg.2017.04.004 [PubMed: 28475860]

Cao R, Wang L, Wang H, Xia L, Erdjument-Bromage H, Tempst P, Jones RS, & Zhang Y (2002). Role of histone H3 lysine 27 methylation in Polycomb-group silencing. Science, 298(5595), 1039–1043. 10.1126/science.1076997 [PubMed: 12351676]

Cappuccio G, Ugga L, Parrini E, D'Amico A, & Brunetti-Pierri N (2019). Severe presentation and complex brain malformations in an individual carrying a CCND2 variant. Molecular Genetics & Genomic Medicine, 7(6), e708. 10.1002/mgg3.708 [PubMed: 31056854]

Chen CP, Lin SP, Chern SR, Wu PS, Chang SD, Ng SH, Liu YP, Su JW, & Wang W (2012). A de novo 4.4-Mb microdeletion in 2p24.3→p24.2 in a girl with bilateral hearing impairment, microcephaly, digit abnormalities and Feingold syndrome. European Journal of Medical Genetics, 55(11), 666–669. 10.1016/j.ejmg.2012.07.003 [PubMed: 22842076]

Choufani S, Cytrynbaum C, Chung BH, Turinsky AL, Grafodatskaya D, Chen YA, Cohen AS, Dupuis L, Butcher DT, Siu MT, Luk HM, Lo IF, Lam ST, Caluseriu O, Stavropoulos DJ, Reardon W, Mendoza-Londono R, Brudno M, Gibson WT, … Weksberg R (2015). NSD1 mutations generate a genome-wide DNA methylation signature. Nature Communications, 6, 10207. 10.1038/ncomms10207

Choufani S, Gibson WT, Turinsky AL, Chung BHY, Wang T, Garg K, Vitriolo A, Cohen ASA, Cyrus S, Goodman S, Chater-Diehl E, Brzezinski J, Brudno M, Ming LH, White SM, Lynch SA, Clericuzio C, Temple IK, Flinter F, … Weksberg R (2020). DNA methylation signature for EZH2 functionally classifies sequence variants in three PRC2 complex genes. American Journal of Human Genetics, 106(5), 596–610. 10.1016/j.ajhg.2020.03.008 [PubMed: 32243864]

Chung BK, Eydoux P, Van Karnebeek CD, & Gibson WT (2014). Duplication of AKT3 is associated with macrocephaly and speech delay. American Journal of Medical Genetics. Part A, 164A(7), 1868–1869. 10.1002/ajmg.a.36521 [PubMed: 24700746]

Cohen AS, & Gibson WT (2016). EED-associated overgrowth in a second male patient. Journal of Human Genetics, 61(9), 831–834. 10.1038/jhg.2016.51 [PubMed: 27193220]

Cohen AS, Yap DB, Lewis ME, Chijiwa C, Ramos-Arroyo MA, Tkachenko N, Milano V, Fradin M, McKinnon ML, Townsend KN, Xu J, Van Allen MI, Ross CJD, Dobyns WB, Weaver DD, & Gibson WT (2016). Weaver syndrome-associated EZH2 protein variants show impaired histone methyltransferase function in vitro. Human Mutation, 37(3), 301–307. 10.1002/humu.22946 [PubMed: 26694085]

Cohen P, & Frame S (2001). The renaissance of GSK3. Nature Reviews. Molecular Cell Biology, 2(10), 769–776. 10.1038/35096075 [PubMed: 11584304]

Conti V, Pantaleo M, Barba C, Baroni G, Mei D, Buccoliero AM, Giglio S, Giordano F, Baek ST, Gleeson JG, & Guerrini R (2015). Focal dysplasia of the cerebral cortex and infantile spasms associated with somatic 1q21.1-q44 duplication including the AKT3 gene. Clinical Genetics, 88(3), 241–247. 10.1111/cge.12476 [PubMed: 25091978]

Dardenne E, Beltran H, Benelli M, Gayvert K, Berger A, Puca L, Cyrta J, Sboner A, Noorzad Z, MacDonald T, Cheung C, Yuen KS, Gao D, Chen Y, Eilers M, Mosquera JM, Robinson BD, Elemento O, Rubin MA, … Rickman DS (2016). N-Myc induces an EZH2-mediated transcriptional program driving neuroendocrine prostate cancer. Cancer Cell, 30(4), 563–577. 10.1016/j.ccell.2016.09.005 [PubMed: 27728805]

de Pontual L, Yao E, Callier P, Faivre L, Drouin V, Cariou S, Van Haeringen A, Geneviève D, Goldenberg A, Oufadem M, Manouvrier S, Munnich A, Vidigal JA, Vekemans M, Lyonnet S, Henrion-Caude A, Ventura A, & Amiel J (2011). Germline deletion of the miR-17 approximately 92 cluster causes skeletal and growth defects in humans. Nature Genetics, 43(10), 1026–1030. 10.1038/ng.915 [PubMed: 21892160]

Diez H, Garrido JJ, & Wandosell F (2012). Specific roles of Akt iso forms in apoptosis and axon growth regulation in neurons. PLoS One, 7 (4), e32715. 10.1371/journal.pone.0032715 [PubMed: 22509246]

Dikow N, Maas B, Gaspar H, Kreiss-Nachtsheim M, Engels H, Kuechler A, Garbes L, Netzer C, Neuhann TM, Koehler U, Casteels K, Devriendt K, Janssen JWG, Jauch A, Hinderhofer K, & Moog U (2013). The phenotypic spectrum of duplication 5q35.2-q35.3 encompassing NSD1: Is it really a reversed Sotos syndrome? American Journal of Medical Genetics. Part A, 161A(9), 2158–2166. 10.1002/ajmg.a.36046 [PubMed: 23913520]

Dobyns WB, & Mirzaa GM (2019). Megalencephaly syndromes associated with mutations of core components of the PI3K-AKT-MTOR pathway: PIK3CA, PIK3R2, AKT3, and MTOR. American Journal of Medical Genetics. Part C, Seminars in Medical Genetics, 181, 582–590. 10.1002/ajmg.c.31736

Easton RM, Cho H, Roovers K, Shineman DW, Mizrahi M, Forman MS, Lee VMY, Szabolcs M, De Jong R, Oltersdorf T, Ludwig T, Efstratiadis A, & Birnbaum MJ (2005). Role for Akt3/protein kinase Bgamma in attainment of normal brain size. Molecular and Cellular Biology, 25(5), 1869–1878. 10.1128/MCB.25.5.1869-1878.2005 [PubMed: 15713641]

Eisenman RN (2001). Deconstructing myc. Genes & Development, 15(16), 2023–2030. https://doi.org/10.1101/gad928101 [PubMed: 11511533]

Ersahin T, Tuncbag N, & Cetin-Atalay R (2015). The PI3K/AKT/mTOR interactive pathway. Molecular BioSystems, 11(7), 1946–1954. 10.1039/c5mb00101c [PubMed: 25924008]

Fagerberg L, Hallstrom BM, Oksvold P, Kampf C, Djureinovic D, Odeberg J, Habuka M, Tahmasebpoor S, Danielsson A, Edlund K, Asplund A, Sjöstedt E, Lundberg E, Szigyarto CA, Skogs M, Takanen JO, Berling H, Tegel H, Mulder J, … Uhlén M (2014). Analysis of the human tissue-specific expression by genome-wide integration of transcriptomics and antibody-based proteomics. Molecular & Cellular Proteomics, 13(2), 397–406. 10.1074/mcp.M113.035600 [PubMed: 24309898]

Firth HV, Richards SM, Bevan AP, Clayton S, Corpas M, Rajan D, van Vooren S, Moreau Y, Pettett RM, & Carter NP (2009). DECI-PHER: Database of Chromosomal Imbalance and Phenotype in Humans using Ensembl Resources. https://doi.org/10/1016/j.ajhg.2009.03.010

Franco LM, de Ravel T, Graham BH, Frenkel SM, Van Driessche J, Stankiewicz P, Lupski JR, Vermeesch JR, & Cheung SW (2010). A syndrome of short stature, microcephaly and speech delay is associated with duplications reciprocal to the common Sotos syndrome deletion. European Journal of Human Genetics, 18(2), 258–261. 10.1038/ejhg.2009.164 [PubMed: 19844260]

Gai D, Haan E, Scholar M, Nicholl J, & Yu S (2015). Phenotypes of AKT3 deletion: A case report and literature review. American Journal of Medical Genetics. Part A, 167A(1), 174–179. 10.1002/ajmg.a.36710 [PubMed: 25424989]

Galaktionov K, Chen X, & Beach D (1996). Cdc25 cell-cycle phosphatase as a target of c-myc. Nature, 382(6591), 511–517. 10.1038/382511a0 [PubMed: 8700224]

Garthe A, Huang Z, Kaczmarek L, Filipkowski RK, & Kempermann G (2014). Not all water mazes are created equal: Cyclin D2 knockout mice with constitutively suppressed adult hippocampal neurogenesis do show specific spatial learning deficits. Genes, Brain, and Behavior, 13 (4), 357–364. 10.1111/gbb.12130

Gibson WT, Hood RL, Zhan SH, Bulman DE, Fejes AP, Moore R, Mungall AJ, Eydoux P, Babul-Hirji R, An J, Marra MA, FORGE Canada Consortium, Chitayat D, Boycott KM, Weaver DD, & Jones

SJ (2012). Mutations in EZH2 cause Weaver syndrome. American Journal of Human Genetics, 90(1), 110–118. 10.1016/j.ajhg.2011.11.018 [PubMed: 22177091]

Glickstein SB, Moore H, Slowinska B, Racchumi J, Suh M, Chuhma N, & Ross ME (2007). Selective cortical interneuron and GABA deficits in cyclin D2-null mice. Development, 134(22), 4083–4093. 10.1242/dev.008524 [PubMed: 17965053]

Gorlin RJ, Cohen MM Jr., Condon LM, & Burke BA (1992). Bannayan–Riley–Ruvalcaba syndrome. American Journal of Medical Genetics, 44(3), 307–314. 10.1002/ajmg.1320440309 [PubMed: 1336932]

Grabinski N, Bartkowiak K, Grupp K, Brandt B, Pantel K, & Jucker M (2011). Distinct functional roles of Akt isoforms for proliferation, survival, migration and EGF-mediated signalling in lung cancer derived disseminated tumor cells. Cellular Signalling, 23(12), 1952–1960. 10.1016/j.cellsig.2011.07.003 [PubMed: 21777670]

Graham SE, Tweedy SE, & Carlson HA (2016). Dynamic behavior of the post-SET loop region of NSD1: Implications for histone binding and drug development. Protein Science, 25(5), 1021–1029. 10.1002/pro.2912 [PubMed: 26940890]

Grissom NM, & Reyes TM (2013). Gestational overgrowth and undergrowth affect neurodevelopment: Similarities and differences from behavior to epigenetics. International Journal of Developmental Neuroscience, 31(6), 406–414. 10.1016/j.ijdevneu.2012.11.006 [PubMed: 23201144]

Gulsuner S, Walsh T, Watts AC, Lee MK, Thornton AM, Casadei S, Rippey C, Shahin H, Consortium on the Genetics of Schizophrenia (COGS), PAARTNERS Study Group, Nimgaonkar VL, Go RC, Savage RM, Swerdlow NR, Gur RE, Braff DL, King MC, & McClellan JM (2013). Spatial and temporal mapping of de novo mutations in schizophrenia to a fetal prefrontal cortical network. Cell, 154(3), 518–529. 10.1016/j.cell.2013.06.049 [PubMed: 23911319]

Han YC, Vidigal JA, Mu P, Yao E, Singh I, Gonzalez AJ, Concepcion CP, Bonetti C, Ogrodowski P, Carver B, Selleri L, Betel D, Leslie C, & Ventura A (2015). An allelic series of miR-17 approximately 92-mutant mice uncovers functional specialization and cooperation among members of a microRNA polycistron. Nature Genetics, 47(7), 766–775. 10.1038/ng.3321 [PubMed: 26029871]

Harada A, Miya F, Utsunomiya H, Kato M, Yamanaka T, Tsunoda T, Kosaki K, Kanemura Y, & Yamasaki M (2015). Sudden death in a case of megalencephaly capillary malformation associated with a de novo mutation in AKT3. Child's Nervous System, 31(3), 465–471. 10.1007/s00381-014-2589-y

Hemming IA, Forrest AR, Shipman P, Woodward KJ, Walsh P, Ravine DG, & Heng JI (2016). Reinforcing the association between distal 1q CNVs and structural brain disorder: A case of a complex 1q43-q44 CNV and a review of the literature. American Journal of Medical Genetics. Part B, Neuropsychiatric Genetics, 171B(3), 458–467. 10.1002/ajmg.b.32427

Henriksson M, & Luscher B (1996). Proteins of the Myc network: Essential regulators of cell growth and differentiation. Advances in Cancer Research, 68, 109–182. [PubMed: 8712067]

Herman GE, Butter E, Enrile B, Pastore M, Prior TW, & Sommer A (2007). Increasing knowledge of PTEN germline mutations: Two additional patients with autism and macrocephaly. American Journal of Medical Genetics. Part A, 143A(6), 589–593. 10.1002/ajmg.a.31619 [PubMed: 17286265]

Hermida MA, Dinesh Kumar J, & Leslie NR (2017). GSK3 and its interactions with the PI3K/AKT/mTOR signalling network. Advances in Biological Regulation, 65, 5–15. 10.1016/j.jbior.2017.06.003 [PubMed: 28712664]

Hers I, Vincent EE, & Tavare JM (2011). Akt signalling in health and disease. Cellular Signalling, 23(10), 1515–1527. 10.1016/j.cellsig.2011.05.004 [PubMed: 21620960]

Higashi M, Sakai K, Fumino S, Aoi S, Furukawa T, & Tajiri T (2019). The roles played by the MYCN, Trk, and ALK genes in neuroblastoma and neural development. Surgery Today, 49(9), 721–727. 10.1007/s00595-019-01790-0 [PubMed: 30848386]

Hiraiwa A, Matsui K, Nakayama Y, Komatsubara T, Magara S, Kobayashi Y, Hojo M, Kato M, Yamamoto T, & Tohyama J (2021). Polymicrogyria with calcification in Pallister-Killian syndrome detected by microarray analysis. Brain Dev, 43(3), 448–453. 10.1016/j.braindev.2020.11.003 [PubMed: 33229101]

Huard JM, Forster CC, Carter ML, Sicinski P, & Ross ME (1999). Cerebellar histogenesis is disturbed in mice lacking cyclin D2. Development, 126(9), 1927–1935. [PubMed: 10101126]

Hung CS, Wang S, Yen YT, Lee TH, Wen WC, & Lin RK (2018). Hypermethylation of CCND2 in lung and breast cancer is a potential biomarker and drug target. International Journal of Molecular Sciences, 19(10), 3096. 10.3390/ijms19103096

Igarashi A, Itoh K, Yamada T, Adachi Y, Kato T, Murata D, Sesaki H, & Iijima M (2018). Nuclear PTEN deficiency causes microcephaly with decreased neuronal soma size and increased seizure susceptibility. The Journal of Biological Chemistry, 293(24), 9292–9300. 10.1074/jbc.RA118.002356 [PubMed: 29735527]

Jamuar SS, Lam AT, Kircher M, D'Gama AM, Wang J, Barry BJ, Zhang X, Hill RS, Partlow JN, Rozzo A, Servattalab S, Mehta BK, Topcu M, Amrom D, Andermann E, Dan B, Parrini E, Guerrini R, Scheffer IE, … Walsh CA (2014). Somatic mutations in cerebral cortical malformations. The New England Journal of Medicine, 371(8), 733–743. 10.1056/NEJMoa1314432 [PubMed: 25140959]

Jansen LA, Mirzaa GM, Ishak GE, O'Roak BJ, Hiatt JB, Roden WH, Gunter SA, Christian SL, Collins S, Adams C, Riviére JB, St-Onge J, Ojemann JG, Shendure J, Hevner RF, & Dobyns WB (2015). PI3K/AKT pathway mutations cause a spectrum of brain malformations from megalencephaly to focal cortical dysplasia. Brain, 138(Pt 6), 1613–1628. 10.1093/brain/awv045 [PubMed: 25722288]

Jeong OS, Chae YC, Jung H, Park SC, Cho SJ, Kook H, & Seo S (2016). Long noncoding RNA linc00598 regulates CCND2 transcription and modulates the G1 checkpoint. Scientific Reports, 6, 32172. 10.1038/srep32172 [PubMed: 27572135]

Karczewski KJ, Francioli LC, Tiao G, Cummings BB, Alfoldi J, Wang Q, Collins RL, Laricchia KM, Ganna A, Birnbaum DP, Gauthier LD, Brand H, Solomonson M, Watts NA, Rhodes D, Singer-Berk M, England EM, Seaby EG, Kosmicki JA, … MacArthur DG (2020). The mutational constraint spectrum quantified from variation in 141,456 humans. Nature, 581 (7809), 434–443. 10.1038/s41586-020-2308-7 [PubMed: 32461654]

Kato K, Miya F, Hamada N, Negishi Y, Narumi-Kishimoto Y, Ozawa H, Ito H, Hori I, Hattori A, Okamoto N, Kato M, Tsunoda T, Kanemura Y, Kosaki K, Takahashi Y, Nagata KI, & Saitoh S (2018). MYCN de novo gain-of-function mutation in a patient with a novel megalencephaly syndrome. Journal of Medical Genetics, 56, 388–395. 10.1136/jmedgenet-2018-105487 [PubMed: 30573562]

Kircher M, Witten DM, Jain P, O'Roak BJ, Cooper GM, & Shendure J (2014). A general framework for estimating the relative pathogenicity of human genetic variants. Nature Genetics, 46(3), 310–315. 10.1038/ng.2892 [PubMed: 24487276]

Knoepfler PS, Cheng PF, & Eisenman RN (2002). N-myc is essential during neurogenesis for the rapid expansion of progenitor cell populations and the inhibition of neuronal differentiation. Genes & Development, 16(20), 2699–2712. 10.1101/gad.1021202 [PubMed: 12381668]

Kondratiuk I, Plucinska G, Miszczuk D, Wozniak G, Szydlowska K, Kaczmarek L, Filipkowski RK, & Lukasiuk K (2015). Epileptogenesis following kainic acid-induced status epilepticus in cyclin D2 knock-out mice with diminished adult neurogenesis. PLoS One, 10(5), e0128285. 10.1371/journal.pone.0128285 [PubMed: 26020770]

Kurotaki N, Imaizumi K, Harada N, Masuno M, Kondoh T, Nagai T, Ohashi H, Naritomi K, Tsukahara M, Makita Y, Sugimoto T, Sonoda T, Hasegawa T, Chinen Y, Tomita HA, Kinoshita A, Mizuguchi T, Yoshiura KI, Ohta T, … Matsumoto N (2002). Haploinsufficiency of NSD1 causes Sotos syndrome. Nature Genetics, 30(4), 365–366. 10.1038/ng863 [PubMed: 11896389]

Kwon CH, Luikart BW, Powell CM, Zhou J, Matheny SA, Zhang W, Li Y, Baker SJ, & Parada LF (2006). Pten regulates neuronal arborization and social interaction in mice. Neuron, 50(3), 377–388. 10.1016/j.neuron.2006.03.023 [PubMed: 16675393]

Kwon CH, Zhu X, Zhang J, & Baker SJ (2003). mTor is required for hypertrophy of Pten-deficient neuronal soma in vivo. Proceedings of the National Academy of Sciences of the United States of America, 100 (22), 12923–12928. 10.1073/pnas.2132711100 [PubMed: 14534328]

Kwon CH, Zhu X, Zhang J, Knoop LL, Tharp R, Smeyne RJ, Eberhart CG, Burger PC, & Baker SJ (2001). Pten regulates neuronal soma size: A mouse model of Lhermitte–Duclos disease. Nature Genetics, 29(4), 404–411. 10.1038/ng781 [PubMed: 11726927]

Lee JH, Huynh M, Silhavy JL, Kim S, Dixon-Salazar T, Heiberg A, Scott E, Bafna V, Hill KJ, Collazo A, Funari V, Russ C, Gabriel SB, Mathern GW, & Gleeson JG (2012). De novo somatic mutations in components of the PI3K-AKT3-mTOR pathway cause hemimegalencephaly. Nature Genetics, 44(8), 941–945. 10.1038/ng.2329 [PubMed: 22729223]

Lek M, Karczewski KJ, Minikel EV, Samocha KE, Banks E, Fennell T, O'Donnell-Luria AH, Ware JS, Hill AJ, Cummings BB, Tukiainen T, Birnbaum DP, Kosmicki JA, Duncan LE, Estrada K, Zhao F, Zou J, Pierce-Hoffman E, Berghout J, … Exome Aggregation Consortium (2016). Analysis of protein-coding genetic variation in 60,706 humans. Nature, 536(7616), 285–291. 10.1038/nature19057 [PubMed: 27535533]

Leone G, Sears R, Huang E, Rempel R, Nuckolls F, Park CH, Giangrande P, Wu L, Saavedra HI, Field SJ, Thompson MA, Yang H, Fujiwara Y, Greenberg ME, Orkin S, Smith C, & Nevins JR (2001). Myc requires distinct E2F activities to induce S phase and apoptosis. Molecular Cell, 8(1), 105–113. [PubMed: 11511364]

Leyser M, Dias BL, Coelho AL, Vasconcelos M, & Nascimento OJ (2016). 12p deletion spectrum syndrome: A new case report reinforces the evidence regarding the potential relationship to autism spectrum disorder and related developmental impairments. Molecular Cytogenetics, 9, 75. 10.1186/s13039-016-0278-0 [PubMed: 27708715]

Ling Wang DH, Jiang Z, Luo Y, Norris C, Zhang M, Tian X, & Tang Y (2017). Akt3 is responsible for the survival and proliferation of embryonic stem cells. Biol Open, 6(6), 850–861. [PubMed: 28483982]

Lopes F, Torres F, Soares G, van Karnebeek CD, Martins C, Antunes D, Silva J, Muttucomaroe L, Botelho LF, Sousa S, Rendeiro P, Tavares P, Van Esch H, Rajcan-Separovic E, & Maciel P (2019). The role of AKT3 copy number changes in brain abnormalities and neurodevelopmental disorders: Four new cases and literature review. Frontiers in Genetics, 10, 58. 10.3389/fgene.2019.00058 [PubMed: 30853971]

Lucio-Eterovic AK, Singh MM, Gardner JE, Veerappan CS, Rice JC, & Carpenter PB (2010). Role for the nuclear receptor-binding SET domain protein 1 (NSD1) methyltransferase in coordinating lysine 36 methylation at histone 3 with RNA polymerase II function. Proceedings of the National Academy of Sciences of the United States of America, 107(39), 16952–16957. 10.1073/pnas.1002653107 [PubMed: 20837538]

Lui JC, Barnes KM, Dong L, Yue S, Graber E, Rapaport R, Dauber A, Nilsson O, & Baron J (2018). Ezh2 mutations found in the weaver overgrowth syndrome cause a partial loss of H3K27 histone methyltransferase activity. The Journal of Clinical Endocrinology and Metabolism, 103(4), 1470–1478. 10.1210/jc.2017-01948 [PubMed: 29244146]

Luo A, Cheng D, Yuan S, Li H, Du J, Zhang Y, Yang C, Lin G, Zhang W, & Tan YQ (2018). Maternal interchromosomal insertional translocation leading to 1q43-q44 deletion and duplication in two siblings. Molecular Cytogenetics, 11, 24. 10.1186/s13039-018-0371-7 [PubMed: 29636822]

Marcelis CL, Hol FA, Graham GE, Rieu PN, Kellermayer R, Meijer RP, Lugtenberg D, Scheffer H, van Bokhoven H, Brunner HG, & de Brouwer AP (2008). Genotype–phenotype correlations in MYCN-related Feingold syndrome. Human Mutation, 29(9), 1125–1132. 10.1002/humu.20750 [PubMed: 18470948]

Marsh DJ, Coulon V, Lunetta KL, Rocca-Serra P, Dahia PL, Zheng Z, Liaw D, Caron S, Duboué B, Lin AY, Richardson AL, Bonnetblanc JM, Bressieux JM, Cabarrot-Moreau A, Chompret A, Demange L, Eeles RA, Yahanda AM, Fearon ER, … Eng C (1998). Mutation spectrum and genotype–phenotype analyses in Cowden disease and Bannayan–Zonana syndrome, two hamartoma syndromes with germline PTEN mutation. Human Molecular Genetics, 7(3), 507–515. [PubMed: 9467011]

McMichael G, Bainbridge MN, Haan E, Corbett M, Gardner A, Thompson S, Van Bon BWM, Van Eyk CL, Broadbent J, Reynolds C, O'Callaghan ME, Nguyen LS, Adelson DL, Russo R, Jhangiani S, Doddapaneni H, Muzny DM, Gibbs RA, Gecz J, & MacLennan AH (2015). Whole-exome sequencing points to considerable genetic heterogeneity of cerebral palsy. Molecular Psychiatry, 20(2), 176–182. 10.1038/mp.2014.189 [PubMed: 25666757]

Mercedes Bloch AL, Diplas AA, Pepermans X, Emanuel BS, Rocca MS, Revencu N, & Sznajer Y (2014). Further phenotype description, genotype characterization in patients with de novo

interstitial deletion on 2p23.2–24.1. American Journal of Medical Genetics. Part A, 164A(7), 1789–1794. 10.1002/ajmg.a.36516 [PubMed: 24700699]

Miao L, Yang L, Huang H, Liang F, Ling C, & Hu Y (2016). mTORC1 is necessary but mTORC2 and GSK3beta are inhibitory for AKT3-induced axon regeneration in the central nervous system. eLife, 5, e14908. 10.7554/eLife.14908 [PubMed: 27026523]

Migdalska AM, van der Weyden L, Ismail O, Sanger Mouse Genetics P, Rust AG, Rashid M, White JK, Sánchez-Andrade G, Lupski JR, Logan DW, Arends MJ, & Adams DJ (2012). Generation of the Sotos syndrome deletion in mice. Mammalian Genome, 23(11–12), 749–757. 10.1007/s00335-012-9416-0 [PubMed: 22926222]

Mirzaa GM (1993). MPPH syndrome. In Adams MP, Ardinger HH, Pagon RA, Wallace SE, Bean LJH, Mirzaa GM, & Anemiya A (Eds.), GeneReviews®. Seattle (WA): University of Washington, Seattle.

Mirzaa G, Parry DA, Fry AE, Giamanco KA, Schwartzentruber J, Vanstone M, Logan CV, Roberts N, Johnson CA, Singh S, Kholmanskikh SS, Adams C, Hodge RD, Hevner RF, Bonthron DT, Braun K, Faivre L, Riviére JB, St-Onge J, Gripp KW, … Sheridan EG (2014). De novo CCND2 mutations leading to stabilization of cyclin D2 cause megalencephaly-polymicrogyria-polydactyly-hydrocephalus syndrome. Nature Genetics, 46(5), 510–515. 10.1038/ng.2948 [PubMed: 24705253]

Murai Y, Dobashi Y, Okada E, Ishizawa S, Shiota M, Mori S, & Takano Y (2001). Study on the role of G1 cyclins in Epstein-Barr virus-associated human lymphomas maintained in severe combined immune deficiency (SCID) mice. International Journal of Cancer, 92(2), 232–239. 10.1002/1097-0215(200102)9999:9999<::aid-ijc1171>3.0.co;2-r [PubMed: 11291051]

Mure H, Matsuzaki K, Kitazato KT, Mizobuchi Y, Kuwayama K, Kageji T, & Nagahiro S (2010). Akt2 and Akt3 play a pivotal role in malignant gliomas. Neuro-Oncology, 12(3), 221–232. 10.1093/neuonc/nop026 [PubMed: 20167810]

Muriello M, Kim AY, Sondergaard Schatz K, Beck N, Gunay-Aygun M, & Hoover-Fong JE (2019). Growth hormone deficiency, aortic dilation, and neurocognitive issues in Feingold syndrome 2. American Journal of Medical Genetics. Part A, 179(3), 410–416. 10.1002/ajmg.a.61037 [PubMed: 30672094]

Nakamura K, Kato M, Tohyama J, Shiohama T, Hayasaka K, Nishiyama K, Kodera H, Nakashima M, Tsurusaki Y, Miyake N, Matsumoto N, & Saitsu H (2014). AKT3 and PIK3R2 mutations in two patients with megalencephaly-related syndromes: MCAP and MPPH. Clinical Genetics, 85(4), 396–398. 10.1111/cge.12188 [PubMed: 23745724]

Negishi Y, Miya F, Hattori A, Johmura Y, Nakagawa M, Ando N, Hori I, Togawa T, Aoyama K, Ohashi K, Fukumura S, Mizuno S, Umemura A, Kishimoto Y, Okamoto N, Kato M, Tsunoda T, Yamasaki M, Kanemura Y, … Saitoh S (2017). A combination of genetic and biochemical analyses for the diagnosis of PI3K-AKT-mTOR pathway-associated megalencephaly. BMC Medical Genetics, 18 (1), 4. 10.1186/s12881-016-0363-6 [PubMed: 28086757]

Nellist M, Schot R, Hoogeveen-Westerveld M, Neuteboom RF, van der Louw EJ, Lequin MH, Bindels-de Heus K, Sibbles BJ, de Coo R, Brooks A, & Mancini GM (2015). Germline activating AKT3 mutation associated with megalencephaly, polymicrogyria, epilepsy and hypoglycemia. Molecular Genetics and Metabolism, 114(3), 467–473. 10.1016/j.ymgme.2014.11.018 [PubMed: 25523067]

Oliveira D, Leal GF, Sertie AL, Caires LC Jr., Goulart E, Musso CM, Oliveira J, Krepischi A, Vianna-Morgante AM, & Zatz M (2019). 10q23.31 microduplication encompassing PTEN decreases mTOR signalling activity and is associated with autosomal dominant primary microcephaly. Journal of Medical Genetics, 56(8), 543–547. 10.1136/jmedgenet-2018-105471 [PubMed: 30301738]

Orrico A, Galli L, Buoni S, Orsi A, Vonella G, & Sorrentino V (2009). Novel PTEN mutations in neurodevelopmental disorders and macrocephaly. Clinical Genetics, 75(2), 195–198. 10.1111/j.1399-0004.2008.01074.x [PubMed: 18759867]

Otto T, Horn S, Brockmann M, Eilers U, Schuttrumpf L, Popov N, Kenney AM, Schulte JH, Beijersbergen R, Christiansen H, Berwanger B, & Eilers M (2009). Stabilization of N-Myc is a critical function of Aurora A in human neuroblastoma. Cancer Cell, 15(1), 67–78. 10.1016/j.ccr.2008.12.005 [PubMed: 19111882]

Ouimet B, Pepin E, Bergeron Y, Chagniel L, Beaulieu JM, Massicotte G, & Cyr M (2019). Motor learning deficits and striatal GSK-3 hyperactivity in Akt3 knockout mice. Behavioral Neuroscience, 133(1), 135–143. 10.1037/bne0000292 [PubMed: 30688489]

Poduri A, Evrony GD, Cai X, Elhosary PC, Beroukhim R, Lehtinen MK, Hills LB, Heinzen EL, Hill A, Hill RS, Barry BJ, Bourgeois BFD, Riviello JJ, Barkovich AJ, Black PM, Ligon KL, & Walsh CA (2012). Somatic activation of AKT3 causes hemispheric developmental brain malformations. Neuron, 74(1), 41–48. 10.1016/j.neuron.2012.03.010 [PubMed: 22500628]

Riviere JB, Mirzaa GM, O'Roak BJ, Beddaoui M, Alcantara D, Conway RL, St-Onge J, Schwartzentruber JA, Gripp KW, Nikkel SM, Worthylake T, Sullivan CT, Ward TR, Butler HE, Kramer NA, Albrecht B, Armour CM, Armstrong L, Caluseriu O, … Dobyns WB (2012). De novo germline and postzygotic mutations in AKT3, PIK3R2 and PIK3CA cause a spectrum of related megalencephaly syndromes. Nature Genetics, 44(8), 934–940. 10.1038/ng.2331 [PubMed: 22729224]

Ross ME, Carter ML, & Lee JH (1996). MN20, a D2 cyclin, is transiently expressed in selected neural populations during embryogenesis. The Journal of Neuroscience, 16(1), 210–219. [PubMed: 8613787]

Rushlow DE, Mol BM, Kennett JY, Yee S, Pajovic S, Theriault BL, Prigoda-Lee NL, Spencer C, Dimaras H, Corson TW, Pang R, Massey C, Godbout R, Jiang Z, Zacksenhaus E, Paton K, Moll AC, Houdayer C, Raizis A, … Gallie BL (2013). Characterisation of retinoblastomas without RB1 mutations: Genomic, gene expression, and clinical studies. The Lancet Oncology, 14(4), 327–334. 10.1016/S1470-2045(13)70045-7 [PubMed: 23498719]

Sachwitz J, Meyer R, Fekete G, Spranger S, Matuleviciene A, Kucinskas V, Bach A, Luczay A, Brüchle NO, Eggermann K, Zerres K, Elbracht M, & Eggermann T (2017). NSD1 duplication in Silver–Russell syndrome (SRS): Molecular karyotyping in patients with SRS features. Clinical Genetics, 91(1), 73–78. 10.1111/cge.12803 [PubMed: 27172843]

Schwarz JM, Cooper DN, Schuelke M, & Seelow D (2014). MutationTaster2: Mutation prediction for the deep-sequencing age. Nature Methods, 11(4), 361–362. 10.1038/nmeth.2890 [PubMed: 24681721]

Sellars EA, Zimmerman SL, Smolarek T, & Hopkin RJ (2011). Ventricular noncompaction and absent thumbs in a newborn with tetrasomy 5q35.2–5q35.3: An association with hunter-McAlpine syndrome? American Journal of Medical Genetics. Part A, 155A(6), 1409–1413. 10.1002/ajmg.a.33997 [PubMed: 21567924]

Sherry ST, Ward MH, Kholodov M, Baker J, Phan L, Smigielski EM, & Sirotkin K (2001). dbSNP: The NCBI database of genetic variation. Nucleic Acids Research, 29(1), 308–311. 10.1093/nar/29.1.308 [PubMed: 11125122]

Siavriene E, Preikšaitiene E, Maldžiene Ž, Mikstiene V, Rančelis T, Ambrozaityte L, Gueneau L, Reymond A, & Kučinskas V (2020). A de novo 13q31.3 microduplication encompassing the miR-17 ~92 cluster results in features mirroring those associated with Feingold syndrome 2. Gene, 753, 144816. 10.1016/j.gene.2020.144816 [PubMed: 32473250]

Sicinski P, Donaher JL, Geng Y, Parker SB, Gardner H, Park MY, Robker RL, Richards JAS, McGinnis LK, Biggers JD, Eppig JJ, Bronson RT, Elledge SJ, & Weinberg RA (1996). Cyclin D2 is an FSH-responsive gene involved in gonadal cell proliferation and oncogenesis. Nature, 384(6608), 470–474. 10.1038/384470a0 [PubMed: 8945475]

Sobreira N, Schiettecatte F, Valle D, & Hamosh A (2015). GeneMatcher: A matching tool for connecting investigators with an interest in the same gene. Human Mutation, 36(10), 928–930. 10.1002/humu.22844 [PubMed: 26220891]

Tatton-Brown K, Douglas J, Coleman K, Baujat G, Cole TR, Das S, Horn D, Hughes HE, Temple IK, Faravelli F, Waggoner D, Turkmen S, Cormier-Daire V, Irrthum A, Rahman N, & Childhood Overgrowth Collaboration (2005). Genotype–phenotype associations in Sotos syndrome: An analysis of 266 individuals with NSD1 aberrations. American Journal of Human Genetics, 77(2), 193–204. 10.1086/432082 [PubMed: 15942875]

Tatton-Brown K, Hanks S, Ruark E, Zachariou A, Duarte S, Ramsay E, Snape K, Murray A, Perdeaux ER, Seal S, Loveday C, Banka S, Clericuzio C, Flinter F, Magee A, McConnell V, Patton M, Raith W, Rankin J, … Rahman N (2011). Germline mutations in the oncogene EZH2

cause Weaver syndrome and increased human height. Oncotarget, 2(12), 1127–1133. 10.18632/oncotarget.385 [PubMed: 22190405]

Tatton-Brown K, Murray A, Hanks S, Douglas J, Armstrong R, Banka S, Bird LM, Clericuzio CL, Cormier-Daire V, Cushing T, Flinter F, Jacquemont ML, Joss S, Kinning E, Lynch SA, Magee A, McConnell V, Medeira A, Ozono K, … Rahman N (2013). Weaver syndrome and EZH2 mutations: Clarifying the clinical phenotype. American Journal of Medical Genetics. Part A, 161A(12), 2972–2980. 10.1002/ajmg.a.36229 [PubMed: 24214728]

Tatton-Brown K, & Weksberg R (2013). Molecular mechanisms of childhood overgrowth. American Journal of Medical Genetics. Part C, Seminars in Medical Genetics, 163C(2), 71–75. 10.1002/ajmg.c.31362

Tavana O, Li D, Dai C, Lopez G, Banerjee D, Kon N, Chen C, Califano A, Yamashiro DJ, Sun H, & Gu W (2016). HAUSP deubiquitinates and stabilizes N-Myc in neuroblastoma. Nature Medicine, 22(10), 1180–1186. 10.1038/nm.4180

Tracy B, Graham JM Jr., Feldman G, Perin J, Catherwood A, Knowlton R, Rappaport EF, Emanuel B, Driscoll DA, & Saitta SC (2011). High-resolution genomic arrays identify CNVs that phenocopy the chromosome 22q11.2 deletion syndrome. Human Mutation, 32(1), 91–97. 10.1002/humu.21395 [PubMed: 21120947]

Varga EA, Pastore M, Prior T, Herman GE, & McBride KL (2009). The prevalence of PTEN mutations in a clinical pediatric cohort with autism spectrum disorders, developmental delay, and macrocephaly. Genetics in Medicine, 11(2), 111–117. 10.1097/GIM.0b013e31818fd762 [PubMed: 19265751]

Wang D, Zeesman S, Tarnopolsky MA, & Nowaczyk MJ (2013). Duplication of AKT3 as a cause of macrocephaly in duplication 1q43q44. American Journal of Medical Genetics. Part A, 161A(8), 2016–2019. 10.1002/ajmg.a.35999 [PubMed: 23794269]

Wang JC, Steinraths M, Dang L, Lomax B, Eydoux P, Stockley T, Yong SL, & Van Allen MI (2007). Craniosynostosis associated with distal 5q-trisomy: Further evidence that extra copy of MSX2 gene leads to craniosynostosis. American Journal of Medical Genetics. Part A, 143A(24), 2931–2936. 10.1002/ajmg.a.31946 [PubMed: 17955513]

Wang Z, Xie Y, Zhang L, Zhang H, An X, Wang T, & Meng A (2008). Migratory localization of cyclin D2-Cdk4 complex suggests a spatial regulation of the G1-S transition. Cell Structure and Function, 33(2), 171–183. [PubMed: 18827403]

Xiong Y, Menninger J, Beach D, & Ward DC (1992). Molecular cloning and chromosomal mapping of CCND genes encoding human D-type cyclins. Genomics, 13(3), 575–584. [PubMed: 1386336]

Xue C, Yu DM, Gherardi S, Koach J, Milazzo G, Gamble L, Liu B, Valli E, Russell AJ, London WB, Liu T, Cheung BB, Marshall GM, Perini G, Haber M, & Norris MD (2016). MYCN promotes neuroblastoma malignancy by establishing a regulatory circuit with transcription factor AP4. Oncotarget, 7(34), 54937–54951. 10.18632/oncotarget.10709 [PubMed: 27448979]

Yang ZZ, Tschopp O, Di-Poi N, Bruder E, Baudry A, Dummler B, Wahli W, & Hemmings BA (2005). Dosage-dependent effects of Akt1/protein kinase Balpha (PKBalpha) and Akt3/PKBgamma on thymus, skin, and cardiovascular and nervous system development in mice. Molecular and Cellular Biology, 25(23), 10407–10418. 10.1128/MCB.25.23.10407-10418.2005 [PubMed: 16287854]

Yuen RK, Thiruvahindrapuram B, Merico D, Walker S, Tammimies K, Hoang N, Chrysler C, Nalpathamkalam T, Pellecchia G, Liu Y, Gazzellone MJ, D'Abate L, Deneault E, Howe JL, Liu RS, Thompson A, Zarrei M, Uddin M, Marshall CR, Ring RH, … Scherer SW (2015). Whole-genome sequencing of quartet families with autism spectrum disorder. Nature Medicine, 21(2), 185–191. 10.1038/nm.3792

Zhang H, Lu X, Beasley J, Mulvihill JJ, Liu R, Li S, & Lee JY (2011). Reversed clinical phenotype due to a microduplication of Sotos syndrome region detected by array CGH: Microcephaly, developmental delay and delayed bone age. American Journal of Medical Genetics. Part A, 155A(6), 1374–1378. 10.1002/ajmg.a.33769 [PubMed: 21567906]

Zhou XP, Waite KA, Pilarski R, Hampel H, Fernandez MJ, Bos C, Dasouki M, Feldman GL, Greenberg LA, Ivanovich J, Matloff E, Patterson A, Pierpont ME, Russo D, Nassif NT, & Eng C (2003). Germline PTEN promoter mutations and deletions in Cowden/Bannayan–Riley–Ruvalcaba syndrome result in aberrant PTEN protein and dysregulation of the phosphoinositol-3-

kinase/Akt pathway. American Journal of Human Genetics, 73(2), 404–411. 10.1086/377109 [PubMed: 12844284]

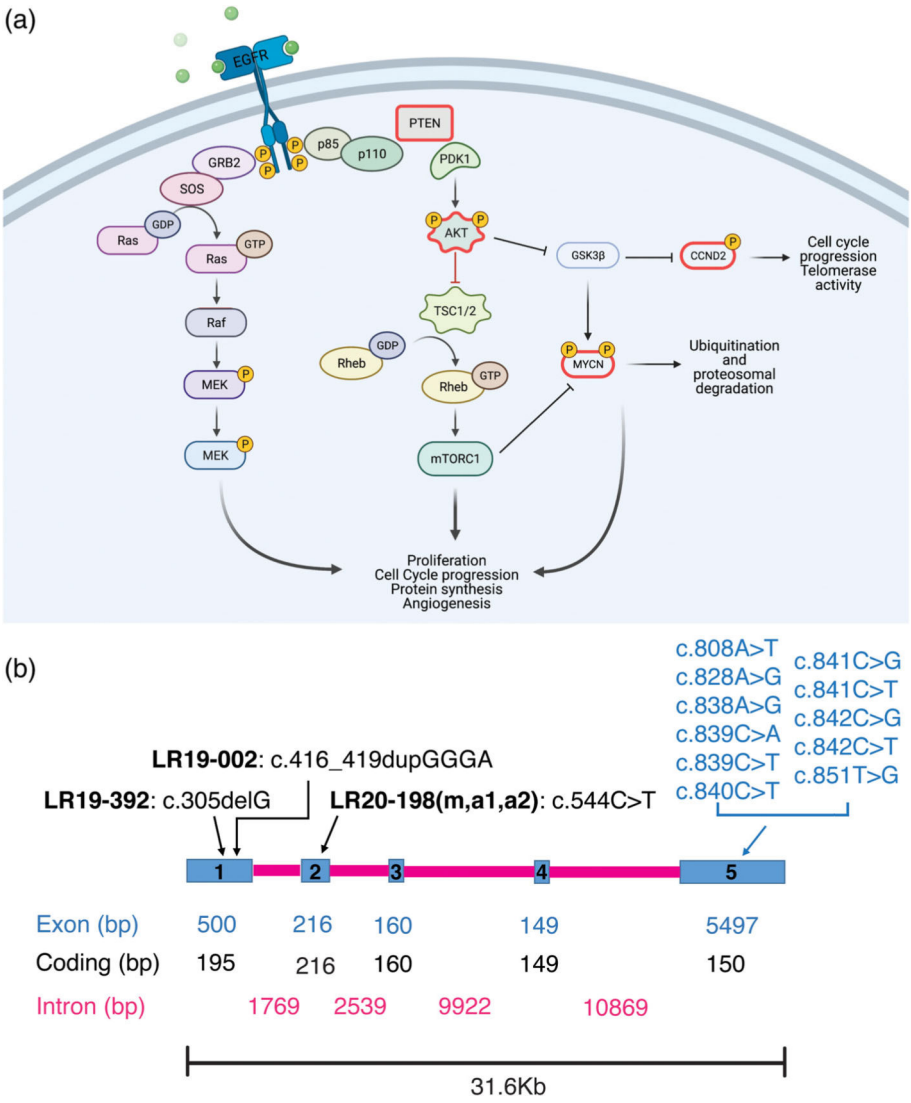

FIGURE 1.

CCND2 gene diagram and role in cell signaling. (a) A schematic representation of the PI3K-AKT-MTOR pathway and its' interaction with the CCND2 protein. Proteins outlined in magenta are the ones with known gain of function and loss of function mutations leading to opposite phenotypes (*PTEN*, *AKT3*, *MYCN*, *CCND2*). Created with BioRender.com. (b) Scheme of the human *CCND2* gene (*Homo sapiens* chromosome 12, GRCh38.p12 CCND2: NC_000012.12 mRNA NM_001759.4 protein NP_001750.1). Blue rectangles represent exons (1–5), while magenta lines represent introns. Exon, coding and intron base pairs length (bp) is shown in the relative colors. Above the gene scheme, putative *CCND2* loss of function (LOF, in black) reported here, and previously published gain of function (GOF, in blue) mutations are reported

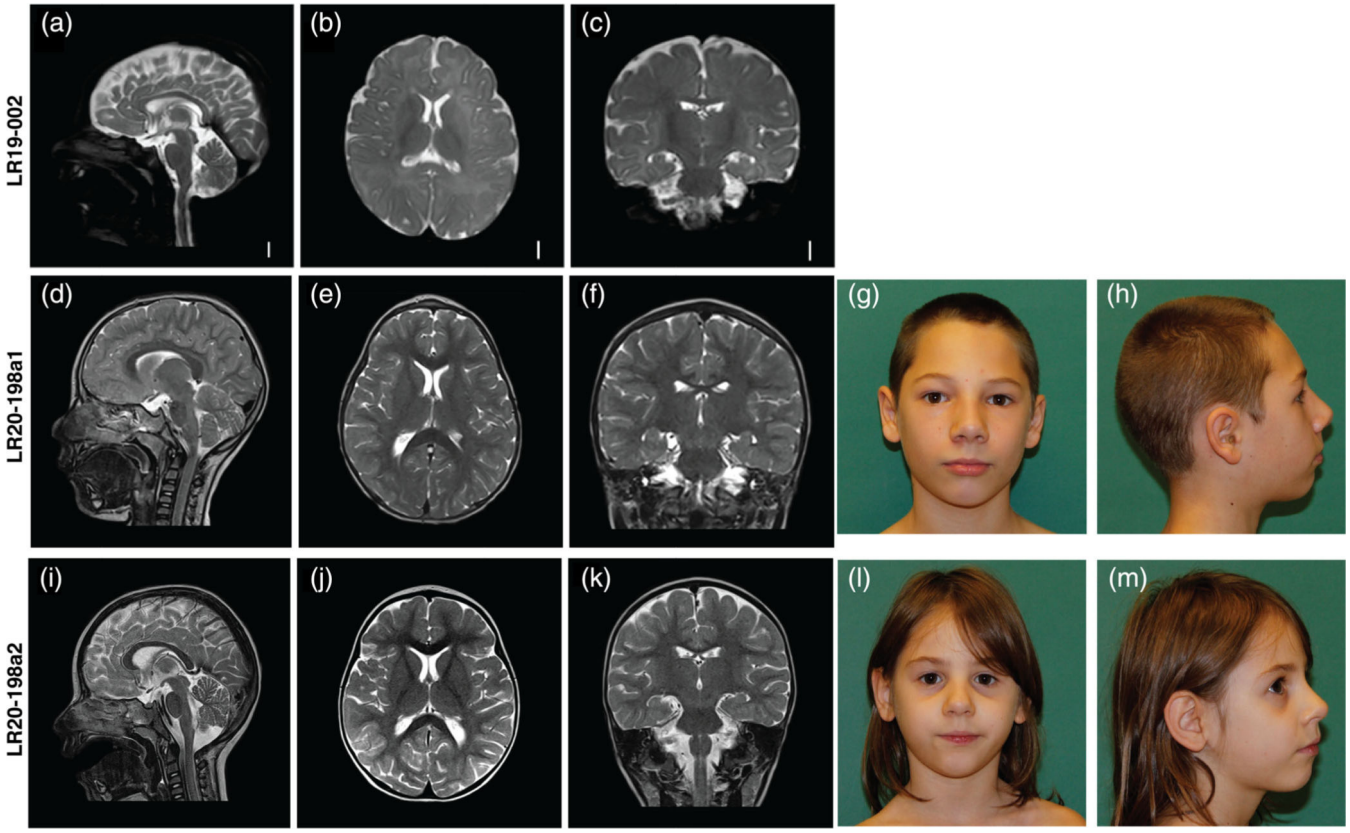

FIGURE 2.

Clinical photographs and brain MR images for three individuals with CCND2-associated microcephaly. (a–c) T2-weighted brain MR images of patient LR19–002 at age 6 months. (a) Midsagittal image showing a mildly thin corpus callosum, with a relatively preserved cerebellar vermis; (b) axial image showing an overall simplified gyral pattern with foreshortened frontal lobes, normal ventricles and (c) coronal image showing also an overall simplified gyral pattern. (d–f) MRI of patient LR20–198a1 at age 4 years showing a mildly foreshortened frontal lobe and subtle simplified gyrification with no cortical malformations and no other major anomalies. (g and h) frontal and lateral pictures of individual LR20–198a1. (i–k) MRI of patient LR20–198a2 at age 2 years 5 months showing a normal appearance with no cortical malformations and no other major anomalies. (l and m) frontal and lateral pictures of patient LR10–198a2

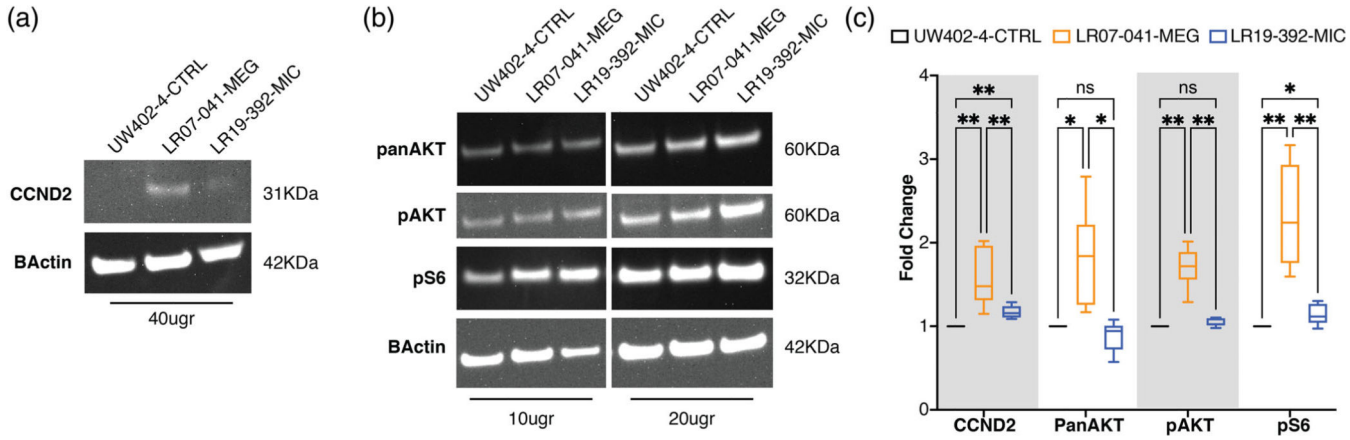

FIGURE 3.

Western blot analysis of MIC- and MEG-associated CCND2 cell lines. Six independent experiments were performed using 10, 20, or 40 μg of protein extracts from fibroblasts cell lines obtained from a wild-type (UW402–4-CTRL), a *CCND2* MIC patient (LR19–392-MIC) and a *CCND2* MEG patient (LR07–041-MEG). (a) Representative blots for CCND2 and beta-actin for the three cell lines, with relative molecular weight shown on the left; due to low expression of CCND2 in fibroblasts, 40 μg of protein extracts was used. (b) Representative blots for PanAKT, pAKT, pS6, and beta-actin for the three cell lines. Two different protein extract concentrations were loaded (10 and 20 μg), the relative molecular weight of each detected protein is shown on the left. (c) Quantification of the analyzed proteins as average of the six independent experiments. The box plot represents the 5–95 centile interval, with the line in the box representing the median value, and the error bars indicating the minimum and maximum value. A one-way ANOVA (mixed effect analysis) was performed to identify significant differences among the cell lines. LR07–041-MEG presented increased expression of CCND2, panAKT, pAKT, and pS6 compared to control. LR19–392-MIC showed increased levels of CCND2 compared to control, but lower than LR07–041. While PanAKT and pAKT were not affected by the increase in CCND2, LR19–392-MIC presented increased levels of pS6 compared to control, albeit at lower levels than LR07–041-MEG. Ns, nonsignificant; **p*-value < 0.05; ***p*-value < 0.01. The full range of quantifications is listed in Supplementary Table 1, additional representative western blots are shown in Supplementary Figure 1

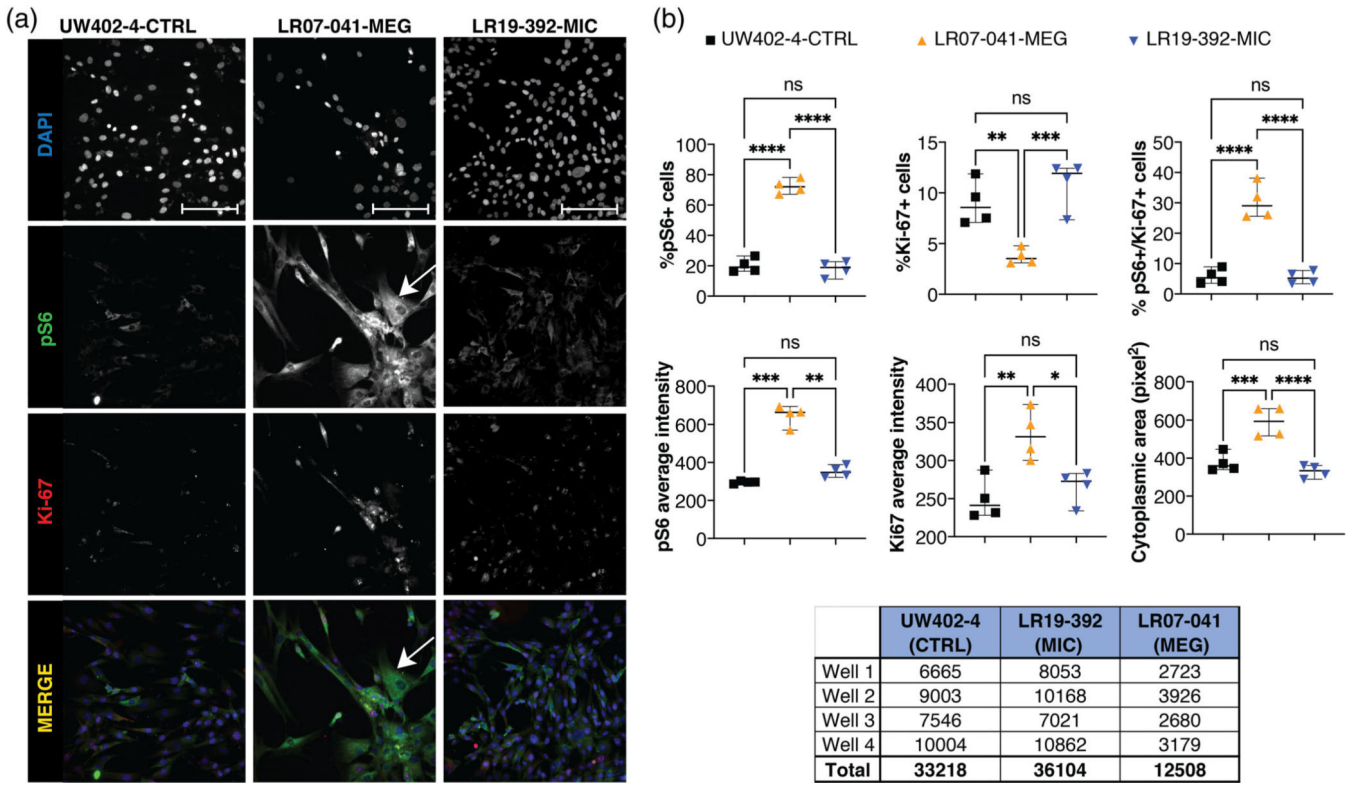

	UW402-4 (CTRL)	LR19-392 (MIC)	LR07-041 (MEG)
Well 1	6665	8053	2723
Well 2	9003	10168	3926
Well 3	7546	7021	2680
Well 4	10004	10862	3179
Total	**33218**	**36104**	**12508**

FIGURE 4.

High-content imaging on fibroblast cell lines with *CCND2* MIC and MEG mutations. Fibroblast cell lines from one control (UW402–4-CTRL), one *CCND2* MIC (LR07–041-MIC), and one *CCND2* MEG (LR19–392-MEG) patients were plated in an optical 96 well plate (4 replicates each) and immunostained for proliferation marker Ki-67 and MTOR hyperactivation marker pS6; nuclei were counterstained with DAPI. Image acquisition and quantification was performed using the high-content imaging platform CellInsight CX7 LZR and the HCS studio software. (a) Single channel and overlay immunofluorescence images of one representative field per well per cell line are shown (20× magnification, scale bar 100 μm). For LR07–041-MEG, a hypertrophic fibroblast is indicated by the white arrow. (b) Quantification of the cells analyzed (4 wells per cell line, 15 fields per well) using the HCS software. Each value represents the average per well per cell line. In each graph and for each cell line, the thick bar represents the median, and the error bars represent the 95% confidence interval. One-way ANOVA analysis with multiple comparison was performed using GraphPad Prism software. Ns, nonsignificant; **p*-value < 0.05; ***p*-value < 0.01; ****p*-value < 0.0001; *****p*-value < 0.00001. LR07–041-MEG shows increase in the percentage of pS6+ and ps6/Ki-67+ cells, with a reduction of Ki-67+ cells. The same line also presented increased intensity (level of expression) for pS6 and Ki-67, as well as increased cytoplasmic area. LR19–392-MIC did not show any significant difference when compared to the control. The table below panel B lists the number of cells analyzed per well per cell line, and the relative total number of cells per cell line

TABLE 1

A summary of clinical and molecular features of inverse brain growth phenotype due to variants in *CCND2*, *AKT3*, *PTEN*, *NSD1*, *MYCN*, *EZH2*, and *MIR17HG*

Gene	Megalencephaly/ macrocephaly Disease (OMIM)	Protein function	Clinical features	Inheritance	Type of variants	Microcephaly Disease (OMIM)	Protein function	Clinical features	Inheritance	Type of variants
CCND2	MPPH3 (#615938)	Gain	Megalencephaly, postaxial polydactyly, hypotonia, epilepsy, intellectual disability, oromotor dysfunction, polymicrogyria	De novo/AD	Missense, nonsense	Microcephaly	Loss[a]	Microcephaly, symmetric short stature, hypotonia, mild intellectual disability, mild motor delay	*De novo*/AD	Missense, small indels
AKT3	MPPH2 (#615937)	Gain	Megalencephaly, polymicrogyria/ cortical dysplasia, postaxial polydactyly, hypotonia, epilepsy, intellectual disability, oromotor dysfunction, connective tissue laxity, vascular malformations	De novo/AD	Missense, duplication	Postnatal microcephaly	Haploin sufficiency/ loss	Microcephaly, callosal abnormalities, seizures, hypotonia, dysmorphic features	*De novo*/AD	Microdeletion 1q43-q44
PTEN	Cowden syndrome (CS), Bannayan-Riley-Ruvalcaba syndrome (BRRS); Lhermitte-Duclos disease (LDD); (#158350)	Loss	Megalencephaly, facial trichilemmomas, acral keratoses, papillomatous papules, hamartoma, increased risk for breast, thyroid, and endometrial carcinoma; hamartomatous polyps of the gastrointestinal tract, mucocutaneous lesions, developmental delay, lipomas, hemangiomas	De novo/AD	Missense, nonsense, small/ large deletions	Microcephaly	Gain	Primary microcephaly, autism spectrum disorder, intellectual disability	AD	Microduplication 10q23.31

Gene	Megalencephaly/ macrocephaly Disease (OMIM)	Protein function	Clinical features	Inheritance	Type of variants	Microcephaly Disease (OMIM)	Protein function	Clinical features	Inheritance	Type of variants
	Autism spectrum disorder with macrocephaly (#605309)	Loss	Megalencephaly, abnormal facial features, and delayed psychomotor development resulting in autistic behavior or mental retardation	De novo/AD	Missense, nonsense, small/ large deletions					
NSD1	Sotos syndrome (#117550)	Loss	Megalencephaly, somatic overgrowth, dysmorhpic facial features, cardiac issues, skeletal issues, renal anomalies, developmental delay/intellectual disability	De novo/AD	Missenese, nonsense, splicing defects, frameshift, deletions	Microcephaly	Gain	Microcephaly, short stature, seizures, developmental delay/ intellectual disability, dysmorphic facial features	*De novo*/AD	Microduplication 5q35
MYCN	*MYCN* related megalencephaly syndrome	Gain	Brain abnormalities (megalencephaly, ventriculomegaly, hypoplastic corpus callosum); Intellectual disability, polydactyly; neuroblastoma	De novo	Missense (c.173C>T)	Feingold syndrome type 1 (#164280)	Loss	Microcephaly; Limb abnormalities (clinodactyly, syndactyly, thumb hypoplasia); Esophageal and or duodenal atresia; Learning disabilities; Characteristic facial features (micrognathia, short palpebral fissures)	AD/ unknown *de novo*	Nonsense, missense, large deletions, partial and entire gene deletions
EZH2	Weaver syndrome (#277590)	Loss	Megalencephaly, overgrowth, distinctive facial gestalt, accelerated bone maturation, developmental delays	De novo	Missense	Microcephaly and developmental delays	Gain	Growth failure, hypotonia, "clover-leaf" shaped skull, large anterior fontanelle, sparse eyebrows, upslanting palpebral fissures, and small ears, developmental delays	*De novo*	Missense
MIR17HG	*MIR17HG* related overgrowth syndrome	Gain	Megalencephaly, developmental delay, skeletal and digital abnormalities, tall stature	De novo	13q31.3 microduplications	Feingold syndrome type 2 (#614326)	Loss	Microcephaly, brachymesophalangy, toe syndactyly, short stature, cardiac anomalies, growth hormone deficiency, aortic dilation, phalangeal joint	*De novo*	13q31.3 microdeletions

Gene	Megalencephaly/ macrocephaly Disease (OMIM)	Protein function	Clinical features	Inheritance	Type of variants	Microcephaly Disease (OMIM)	Protein function	Clinical features	Inheritance	Type of variants
								contractures, memory, and sleep problems		

Notes: When available, the OMIM number is listed, otherwise the disorder has not yet been described in OMIM.

Abbreviations: AD, autosomal dominant; IUGR, intrauterine growth restriction; MPPH, megalencephaly-polymicrogyria-polydactyly-hydrocephalus syndrome; UK, unknown.

[a]Predicted loss of function due to premature stop codon based on the five cases reported here.

TABLE 2

Summary of clinical and molecular features for individuals with microcephaly and novel *CCND2* variants

		LR19-002	LR19-392	LR20-198 m	LR20-198a1	LR20-198a2
Genetic testing	Identified variant	*CCND2*: NM_001759.4: c.416_419dupGGGA, p.L141GfsX19	*CCND2*: NM_001759.4:c.305delG, p.G102VfsX17	*CCND2*: NM_001759.4:c.544C>T, p.Q182X(het)		
	Molecular methods and other molecular findings [inheritance]	Exome sequencing; GBA (c.882T>G, p.H294Q), het, VUS [pat]; *TENM1* (c.679 C>A, p.P227T), VUS, [mat]	NGS panel; no	Array CGH, targeted sequencing, arr 18q12.3 (37.877.518–37.961.503)x3 (hg18)	Exome sequencing, Array CGH, arr 18q12.3 (37.877.518–37.961.503)x3mat (hgl8)	Array CGH, Targeted sequencing, arr 8q23.1 (106.455.702–107.566.961) x3pat,18q12.3 (37.877.518–37.961.503)x3mat (hgl8)
Demographics	Sex	M	F	F	M	F
	Age at last assessment	7m	12y2m	30y	12y11m	6y8m
	Ethnicity	ND	ND	Caucasian (Germany)	Caucasian (Germany)	Caucasian (Germany)
	Notable family history	Non-consanguineous, conceived via intrauterine insemination, family history unremarkable	Non-consanguineous, family history unremarkable	Father has boderline ID, short stature and microcephaly without genetic diagnosis	See LR20-198 m. One sibling and two maternal half siblings show normal OFC and normal development and do not carry CCND2 variant	See LR20-198a1
Pregnancy and birth	Pregnancy	G1P1 mother, suspected preeclampsia, vaginal bleeding, IUGR at 32-33gw	G2P2, IUGR at end of second trimester	G1P1	G1P1	G4P3
	Gestational age (weeks/days)	35 + 6	39 + 0	ND	38 + 5	37 + 5
	Birth weight (%le/z-score)	1870 g (2.13%, −2.05 SD)	2320 g (3%, −1.8 SD)	ND	2900 g (10–25%, −1.2 SD)	2480 g (3%, −1.8 SD)
	Birth length (%le/z-score)	43.5 cm (3%, −1.8 SD)	46 cm (3–10%, −1.5 SD)	ND	49 cm (25–50%, −1 SD)	47 cm (10–25%, −1.3 SD)
	Birth head circumference (%le/z-score)	30.5 cm (3–10%, −1–2 SD)	32 cm (2%, −2 SD)	ND	29.5 cm (<1%, −4.3 SD)	32 cm (2%, −2 SD)
Growth	Weight at last assessment (%le/z-score)	6.1 kg (0.48%, −2.6 SD)	25.50 kg (<0.1%, −2.8 SD)	85 kg (95%, +1.68 SD)	34.2 kg (5%, −1.7 SD)	15.2 kg (<1%, −2.8 SD)
	Height at last assessment (%le/z-score)	64.5 cm (5%, −1.6 SD)	140.5 cm (7%, −1.4 SD)	150 cm (2%, −2 SD)	144.5 cm (7%, −1.5 SD)	111 cm (2%, −2 SD)

		LR19-002	LR19-392	LR20-198 m	LR20-198a1	LR20-198a2
	Head circumference at last assessment (%1e/z-score)	40.2 cm (<1%, −3.1 SD)	48 cm (<1%, −4.3SD)	51 cm (<1%, −3.1 SD)	48 cm (<1%, −4.2 SD)	45.2 cm (<1%, −5 SD)
	Growth failure	Yes	Yes	Yes	No	Yes
Neurologic findings	Degree of developmental delay or ID	N.E.		Mild	Mild	Mild
	Age–1st walked	N.E.	13 m	2 years	12 month	11 month
	Age–1st words	N.E.		Unknown	Unknown	Unknown
	Speech delays	N.E.	Yes	Unknown	Yes (with 3 years less than 100 words and two-word-sentences)	Yes
	Seizures	No	No	No	No	No
	EEG findings	N.E.	N.E.	N.E.	normal	yes, among others occipital epileptic potentials
	Tone abnormalities	Hypotonia	No	N.E.	No	No
	Brain MRI findings	Microcephaly with a mildly simplified gyral pattern	Microcephaly with a mildly simplified gyral pattern	N.E.	Normal	Normal
	Autism	N.E.	No	N.E.	No	No
	ADHD	N.E.	Yes, mild	N.E.	Suspected	N.E.
	Other behavioral issues	N.E.	No		aggressive, impulsive and antisocial behavior	recurring (breath-holding spells), impusive behavior, reduced interaction with peers
	Other neurologic findings	No	No	No	No	No
	Formal developmental or autism assessments	N.E.	Special school	Attended a special school	Attended a special school	Bayley II (23 month): in the lower standard range
Other findings	Dysmorphic facial features	Mild right occipital flattening	Large ears, short philtrum, incomplete single transverse right palmar crease	Sloping forehead, broad nasal tip, upslanting palpebral fissures, long philtrum, thin upper lip vermilion	Sloping forehead, broad nasal base, broad nasal tip, long philtrum, thin upper lip vermilion	Sloping forehead, broad nasal tip
	Heart	N.E.	N.E.	N.E.	N.E.	N.E.
	Eyes	N.E.	Mild myopia	N.E.	N.E.	Normal
	Urogenital system	N.E.	N.E.	N.E.	N.E.	N.E.
	Skeletal	N.E.	Bone age delayed at 2y10m, normalized later	N.E.	Pes planus	Talus obliqus and pes planus unilateral
	GI	N.E.	N.E.	N.E.	N.E.	Nutritional difficulties

	LR19-002	LR19-392	LR20-198 m	LR20-198a1	LR20-198a2
Other medical issues	Mild motor delays at birth, responded well to physical therapy	No	Bilateral inguinal hernia after birth	Asphyxia, anchyloglossia	Respiratory adaptation disorder with CPAP-therapy, failure to thrive

Notes: The table summarizes the clinical features, growth data, and family history for the five individuals with proximal *CCND2* frameshift or stop-gain variants.

Abbreviation: N.E., not evaluated.

TABLE 3

Analysis of variants pathogenicity and frequency in the population

	Variant			Variant frequency		
Gene	**CDS**	**Protein**	**Mutation Taster**	**dbSNP**	**gnomAD (Mut/ref[a])**	**1000G**
CCND2	c.305delG	p.G102Vfsx17	Disease causing	Not present	0/251466	Not present
CCND2	c.416_419dupGGGA	p.L141GfsX19	Disease causing	Not present	0/249026	Not present
CCND2	c.544C>T	p.Q182X	Disease causing	Not present	0/248742	Not present
GBA	c.882T>G	p.H294Q	Disease causing	Not present	0/279868	Not present
TENM1	c.679C>A	p.P227T	Disease causing	Not present	0/156640	Not present

Notes: Genetic variants found in individuals LR19-002, LR19-392, LR20-198 m, LR20-198a1, and LR20-198a2 are listed with their respective prediction of pathogenicity (Mutation Taster) and frequency in the population based on data collected in dbSNP, gnomAD, and 1000 Genome project (1000G) (results as of April 5, 2021).

[a]For gnomAD reference allele frequency, data for the closest variant in the database were used to estimate the coverage of the region.